

Lawrence Berkeley National Laboratory

Lawrence Berkeley National Laboratory

Title

ANALYSIS OF THE INTERACTION OF 300-Mev NEUTRONS WITH XENON

Permalink

<https://escholarship.org/uc/item/0v69z1mr>

Author

Morris, Richard Herbert.

Publication Date

2009-03-26

UCRL 3603

UNIVERSITY OF
CALIFORNIA

*Radiation
Laboratory*

TWO-WEEK LOAN COPY

*This is a Library Circulating Copy
which may be borrowed for two weeks.
For a personal retention copy, call
Tech. Info. Division, Ext. 5545*

BERKELEY, CALIFORNIA

UCRL-3603

UNIVERSITY OF CALIFORNIA

Radiation Laboratory
Berkeley, California

Contract No. W-7405-eng-48

ANALYSIS OF THE INTERACTION OF 300-Mev NEUTRONS
WITH XENON

Richard Herbert Morris
(Thesis)

October 17, 1956

Printed for the U.S. Atomic Energy Commission

ANALYSIS OF THE INTERACTION OF 300-Mev NEUTRONS
WITH XENON

Contents

Abstract	4
Introduction	5
Experimental Procedure	
Production of Events	
Neutron Beam and Collimation	6
Cloud Chamber and Gas Analysis	6
Magnet and Photography	9
Cycle of Operations	9
Method of Analysis of Events	
Adjustment of Projector	10
Scanning Procedure	10
Measurements	10
Identification	15
Effects of Contamination	17
Results and Discussion	
Meson Events	
Angular Distribution of Mesons	20
Energy Distribution of Mesons	28
Energy of Neutrons Producing Mesons	28
Classification and Analysis of Prongs	
Associated with Mesons	32
Residual Nuclei	41
Events Not Associated with Mesons	
Angular and Energy Distributions of Protons	43
Angular and Energy Distributions of Deuterons	43
Heavier Particles	55
Residual Nuclei	55
Star Yield vs Neutron Energy	55
Azimuthal Symmetry Check	55

Contents (cont.)

Acknowledgments	65
Appendices	
Appendix I.	66
Appendix II.	69
References	70

ANALYSIS OF THE INTERACTION OF 300-Mev NEUTRONS
WITH XENON

Richard Herbert Morris

Radiation Laboratory
University of California
Berkeley, California

October 17, 1956

ABSTRACT

An investigation of the interactions between 300-Mev neutrons and xenon was made by means of a cloud chamber in a pulsed magnetic field of 21,700 gauss placed in the neutron beam of the 184-inch Berkeley cyclotron. Eighty-seven negative pion events and 257 other stars were analyzed. In addition an experimental check was made on the energy of the incoming neutrons. Classification, identification, and angular and energy distributions of prongs associated with all events are presented. Interpretations of results are given.

I. INTRODUCTION

Since the advent of particle accelerators much information has been obtained concerning nucleon-nucleon interactions. The bombardment of heavy nuclei with nucleons has also revealed how fundamental interactions are altered in the presence of nuclear matter.

The work done by the cloud chamber group at this laboratory on the interaction of 300-Mev neutrons with deuterium,¹ helium,² and oxygen^{3,4} has yielded information on both mesons and other stars, and the revelation of important differences associated with a greater atomic weight suggested the practicality of performing a similar experiment with a heavy element.

A heavy element in gaseous form was decided upon, since the use of a gas would permit observation of origins of individual events with smaller turbulence than would be present if plates were used. Consequently the element Xe was chosen. The presence of 77 neutrons and 54 protons in the nucleus of Xe places it intermediate between Ag-Br of nuclear emulsions and Pb.

In the experimental analysis that follows, comparisons are made between events produced by 300-Mev neutrons incident on Xe and those produced by the same neutron beam incident on the lighter elements. Both meson events and other stars are included in this analysis and plausible interpretations have been sought for differences that exceed the statistical errors of the experiment.

II. EXPERIMENTAL PROCEDURE

Production of Events

Neutron Beam and Collimation

A beam of 340-Mev protons incident on a 1-inch-thick LiD target was the source of the high-energy neutrons used in this experiment. (see Fig. 1).

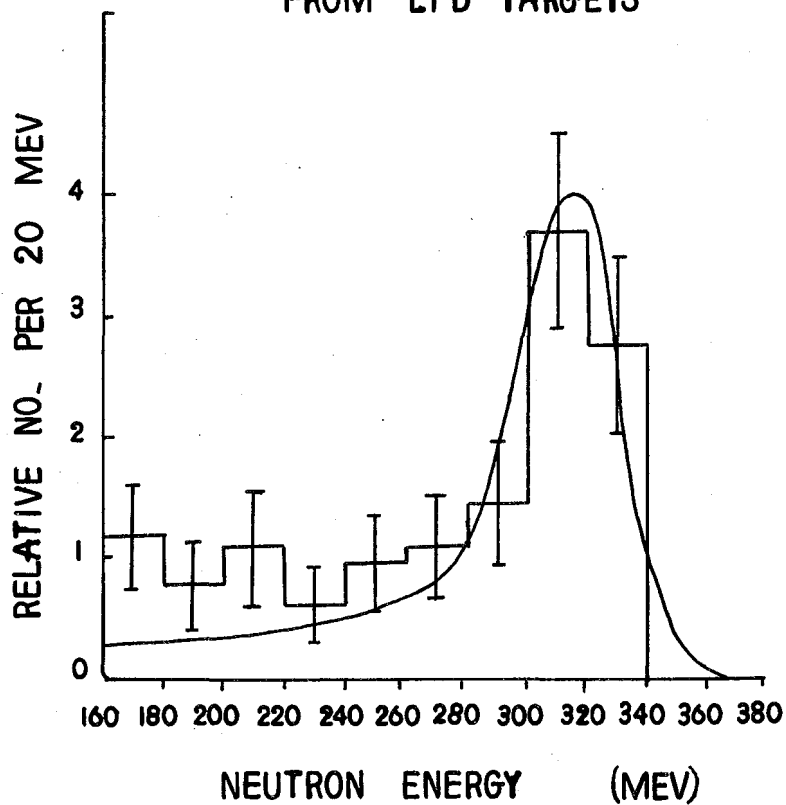
The collimation system was as shown in Fig. 2. The neutrons first passed through a 7-foot-long brass collimator which had one end plugged with a 12-inch piece of paraffin in order to decrease the number of low-energy neutrons in the beam. A second collimator, 3 feet long, was situated at the exit port of the concrete shielding. The beam used for producing events was defined by a third collimator, which was 3 feet long, 1 inch high, and 4-1/8 inches wide. Before entering the cloud chamber the neutrons passed through a thin window consisting of a 3-mil copper foil, 1 inch high and 5 inches wide. The neutrons passed through a second thin window after traversing the cloud chamber in order to reduce the effects of back-scattering.

Cloud Chamber and Gas Analysis

The events were produced in an expansion-type cloud chamber⁵ filled with Xe, H₂, and small amounts of other gases. This chamber had a diameter of 22 inches and a height of 3.5 inches. It was operated with water vapor at an average pressure, in the expanded position, of 22 cm above atmospheric. A circulating water system, maintained at 19.2° C, controlled the temperature of the chamber and reduced gas turbulence. Seven fiducial marks were painted on the top glass of the chamber as an aid both in aligning the chamber along the direction of the neutron beam and in reprojecting the pictures taken of the neutron events.

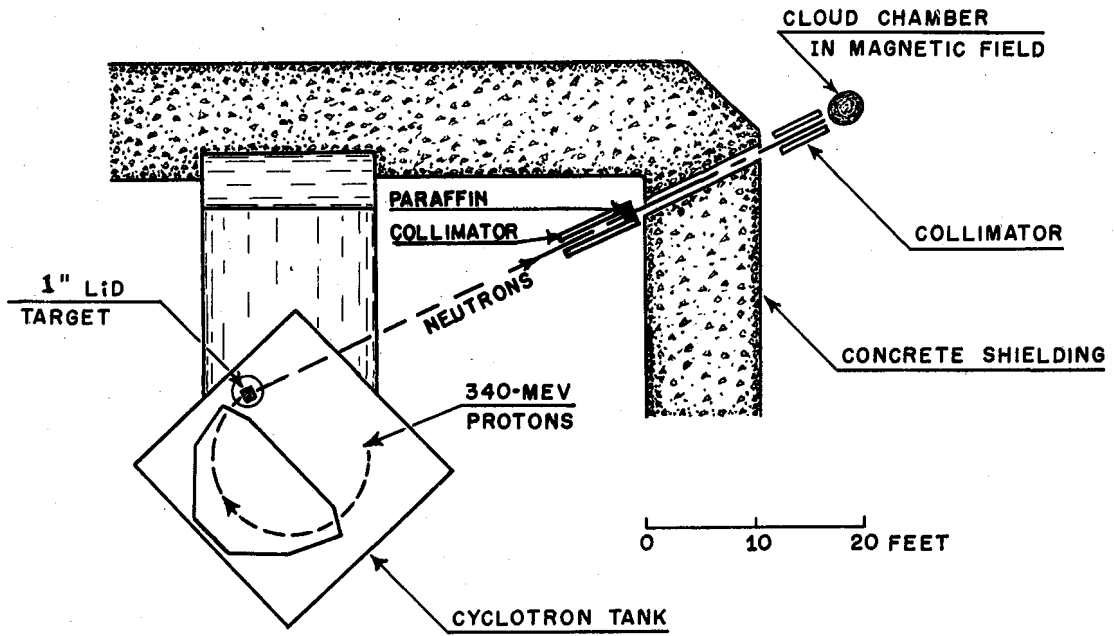
Considerations of multiple scattering and turbulence governed the amount of Xe used, while the presence of hydrogen permitted operation of the chamber near atmospheric pressure and afforded a means of determining the neutron energy spectrum. The actual percentage composition of the gas was determined by means of a mass spectrometer.

NEUTRON-ENERGY SPECTRUM FROM LiD TARGETS



MU-12363

Fig. 1. The uniform curve represents the neutron spectrum obtained from a 0.5-inch LiD target by W. P. Ball. Superimposed on this curve is a histogram of the neutron-energy spectrum obtained from a 1-inch LiD target used in the xenon experiment.



MU-5006-A

Fig. 2. The collimation system.

Three such analyses were made during the course of the experiment, and the average of these three (in mole %) is as follows: Xe, 14.68%; N₂, 0.37%; O₂, 0.20%; H₂O, 0.50%; Kr, 0.04%; C₆H₆, 0.02%; H₂, 84.19%.

The following procedure was used in filling the chamber. It was first flushed with He to remove room air. It was then flushed and filled with H₂ to approximately atmospheric pressure. The Xe gas was allowed to freeze into a small evacuated glass cylinder immersed in liquid nitrogen, one end of the cylinder having been connected to the inlet of the cloud chamber. When the cylinder was removed from the liquid nitrogen, the Xe melted and expanded into the chamber. Four liters of Xe at atmospheric pressure was inserted by this means.

Magnet and Photography

The cloud chamber was situated between the poles of a magnet as shown in Fig. 3; the bottom of the chamber formed a part of the lower pole.⁵ During the experiment the magnet produced a pulsed field which had a maximum value of 21,700 gauss near the center of the cloud chamber. This field varied by no more than 6% from its central value over the region in which events were produced.

Pictures were taken in pairs with a stereoscopic camera situated approximately 27 inches above the top glass of the chamber. Two flash tubes, one on either side of the cloud chamber, served to illuminate the region in which the events were produced and to expose the film in the camera. These tubes were flashed by discharging across each of them a 256-microfarad condenser, charged to 1550 volts.

Cycle of Operations

Each time a picture was taken the following procedure was used. First the current to the magnet was turned on so that its maximum value of 4000 amperes, maintained for approximately 0.15 second, would coincide in time with the expansion of the cloud chamber. Next the clearing-field voltage of 100 volts was turned off. Then expansion of the cloud chamber took place, and at the instant the chamber reached

full expansion the cyclotron was pulsed. After traversal of the beam the lights were flashed, exposing the film in the camera. The clearing field was once again turned on an a period of 1.5 minutes elapsed before the cycle was repeated.

Method of Analysis of Events

Adjustment of Projector

Analysis of events was accomplished by reprojecton on the translucent screen of a double projector, similar to that shown in Fig. 4.⁶ The optical system was quite similar to that of the stereoscopic camera, with the screen placed at a distance from the lenses equal to that between the stereoscopic camera and the top glass of the cloud chamber. Life-size reprojecton of the events was obtained by adjusting the focus of each lens until the distance between the fiducial marks as projected on the screen was equal to the distance between the fiducial marks on the top glass. Translational motion of the two images, accomplished by rotating the film in the holders, permitted accurate superposition of the two images. A final check on the adjustment was made by determining whether the sensitive region of the cloud chamber was in good focus.

Scanning Procedure

The film was first scanned on the projector and all events observed to have originated within the collimated region of the cloud chamber were recorded. A second scan was made by viewing the film through a stereoscopic viewer of high magnification. A trace of the events found on each of these instruments was made and then the two traces were compared as a check on scanning efficiency. Whenever an event was recorded an effort was made to locate a long, well-defined track in the immediate vicinity of the event as an aid in identification. All identification tracks were included in the trace.

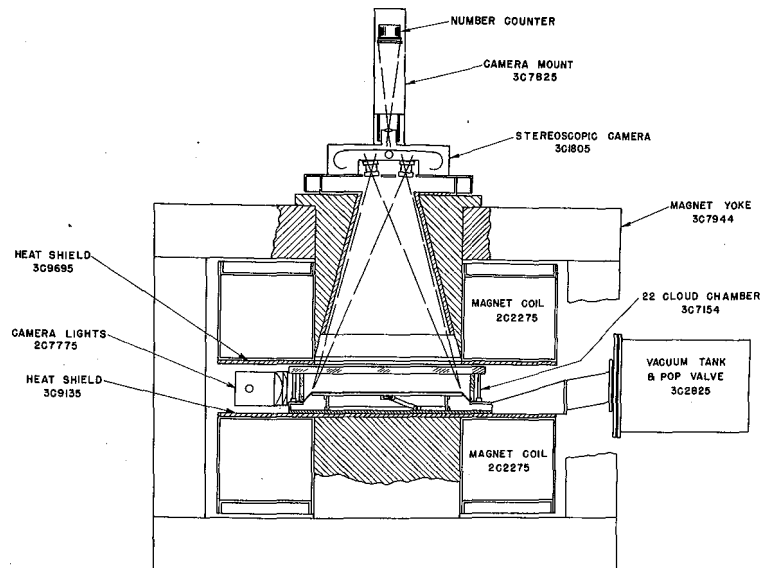


Fig. 3. The cloud chamber and magnet.

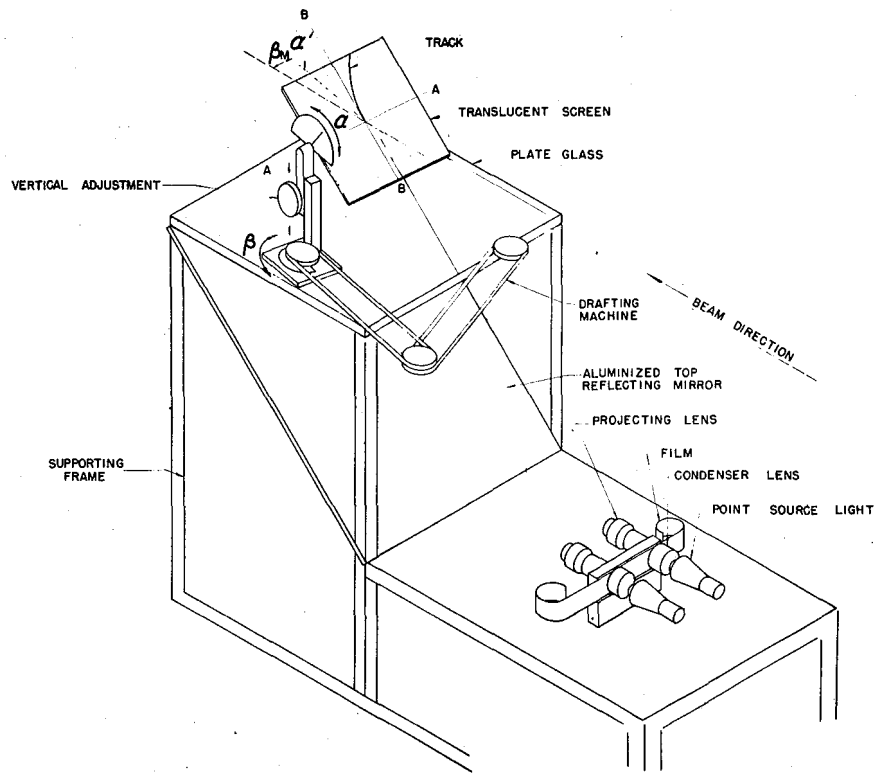


Fig. 4. The stereoscopic projector.

When the film was scanned for meson events, all the precautions mentioned above were taken, and in addition all of the film was scanned by three independent observers. When it was discovered that few mesons were found that were emitted at small angles to the beam direction (see Results and Discussion), another scan was made in which only mesons in the forward direction were sought. No additional events of this nature were found. To determine whether conditions in the chamber were such that condensation on lightly ionizing tracks was sufficient to render them visible, an additional scan was made for high-energy electron-positron pairs. In a total of 736 pictures scanned (those pictures which contained the majority of the identified mesons), 639 pairs were found with an average of almost one per picture. The presence of pairs in such abundance would indicate that the more heavily ionizing tracks of mesons emitted in the forward direction would have been discovered if they had been present.

Measurements

The following data, as measured on the projector, were recorded for each track found in the scanning:

(a) The horizontal region in which the origin of the track occurred. The collimated region of the chamber was divided into 16 rectangular solids of equal depth and lateral area. Distribution of origins in these subvolumes served as a check on scanning efficiency.

(b) The height, H_0 , of the origin of the track. This was obtained by raising or lowering the screen until the two projected images of the origin coincided. The distribution of heights proved useful in determining whether the chamber was tilted with respect to the beam direction.

(c) The dip angle α that the screen makes with the horizontal plane when the screen has been rotated about a horizontal axis until the two projected images of the entire track length coincide. In almost every case the two readings of α taken agreed to within 1° . The actual error in α may be obtained from the published results for the

error in measurement of α : $\pm 1.5^\circ$, $0^\circ < \alpha < 50^\circ$; $\pm 2^\circ$, $\alpha = 60^\circ$; $2-1/2^\circ$, $\alpha > 60^\circ$. The dip angle is used in computing the momentum associated with the track; the angle θ that the track makes with the beam direction; and the azimuthal angle $\overline{\phi}$, defined by the projection of the track direction on a plane perpendicular to the neutron beam and the horizontal plane.

(d) The angle $\underline{\beta}$, measured in the horizontal plane between the direction of the neutron beam and the horizontal projection of the tangent line BB (Fig. 4) when the center of the screen coincides with the origin of the track. For every well-defined track the two values of $\underline{\beta}$ in this experiment agreed to within 1° . Consideration of systematic errors would indicate that the error in determining $\underline{\beta}$ is $\pm 1^\circ$, in agreement with the published results of Wilson Powell.⁶ The angle $\underline{\beta}$ was used in computing both θ and $\overline{\phi}$, and consequently was used when a momentum balance was attempted.

(e) The radius of curvature ρ_s , of the track in the plane of the screen when the screen had been rotated until the two projected images of the entire track were superposed. The value of ρ_s was obtained by attempting to match the track on the projector screen with concentric curves of known radii scribed on a transparent template. In addition to the best matched value of ρ_s , upper and lower limits were recorded. If the track was sufficiently long these measurements were repeated at a second point on the track. The value of ρ_s recorded was used in momentum and energy determinations and the upper and lower limits gave an indication of the error of measurement. In most cases checked the difference between the best matched value and the upper and lower limits of ρ_s was in agreement with the assumption that a constant error of 0.1 mm exists in sagitta measurements. In a few situations the presence of turbulence increased the error.

(f) The length of each track, determined by means of a flexible ruler (the range was recorded if the track stopped in the chamber). The track length was used in investigation of the errors in ρ_s , and the range was used to identify the track and determine its initial energy.

(g) The height of the center of the track above the bottom of the cloud chamber and its distance from the center of the chamber. These values were used to estimate the effective magnetic field acting on the particle.

An analysis, similar to that made above, was made for each track chosen for identification purposes, and for a number of high-energy pairs occurring within the collimated region. The analysis of pairs was made in order to check the alignment of the chamber along the beam direction. The distribution in β obtained from the analysis of pairs indicated that the alignment of the chamber was correct to $\pm 1^\circ$.

In addition, the origin of each event was investigated to determine whether or not a residual was associated with the event. The residuals were found and their ranges measured with the aid of a magnifier provided with a linear scale graduated in tenths of a millimeter. Whenever the residual was long enough, estimates of α and β were made.

Identification

Identification of the various charged particles analyzed in this experiment was made on the basis of ionization, radius of curvature, and rate of change of radius of curvature with range. The ionization estimates were made by comparing event tracks with well-defined background tracks.

For each picture an ionization scale was constructed extending from the region near minimum ionization, consisting of high-energy pairs and knock-on protons from the thin window, to a region several hundred times minimum, consisting of the few low-energy protons that stopped in the chamber. Tracks that stopped in the chamber were determined to be proton tracks by comparison of the experimentally observed endings with the proton endings computed from range-energy values for the known composition of gases in the chamber. The region of the scale between the two extremes mentioned above was constructed

by finding tracks with values of ionization falling within those of known proton tracks. Only tracks that were nearly horizontal ($0^\circ \lesssim \alpha \lesssim 25^\circ$), and which fell within the collimated region of the chamber were accepted for the initial scale. A second scale, consisting of tracks of larger dip angle ($25^\circ < \alpha \lesssim 60^\circ$), was also constructed. The tracks used in this scale were those occurring in the immediate vicinity of known horizontal tracks. More than 400 tracks were used in establishing the first scale and approximately 100 tracks were used in the second one.

The horizontal scale tracks in every picture were found to have certain common characteristics. In the region near minimum the tracks were sparse, and the drop clusters were separated by many gaps. As ionization increased, these clusters became more dense until, in the region of ten times minimum the tracks were just continuous. For still greater values of ionization the thickness increased until in the region of 70 times minimum, the clusters were so dense that the tracks had opaque cores. Track thickness increase gradually above 70 times minimum until a saturation point was reached at ionization values near 200 times minimum.

The smallest ratio of ionization that could be resolved when two tracks of the same radius of curvature were being compared was dependent upon the region of ionization in which the tracks occurred. This ratio was near 1.5 between minimum and ten times minimum; it increased to approximately 2 between 10 and 70 times minimum; and above 70 times minimum no ratios smaller than 3 could be resolved with any certainty.

Event tracks were first identified by use of the projector. The structure of light tracks and thickness of heavy tracks were investigated with the aid of a magnifier, and each eye of the projector was employed. The consistency of these identifications was checked by comparison of each identified track with the other tracks of the event in which it originated. A second identification was made by use of the high-powered viewer, which had the advantage of permitting the events to be viewed stereoscopically with good external illumination.

Little difficulty was encountered in identifying protons, since for the same radius of curvature the smallest ratio of ionization between protons and the other possible charged particles was that between deuterons and protons. The ratio in this case was approximately 3. For small dip angles deuterons could be distinguished from tritons and helium isotopes (He^3) with some reliability over most of the energy range; the ratios in the two cases were about 1.8 and 2.3 respectively. Since the ratio between He^3 and H^3 is about 1.3, no distinction could be made between these two particles. The ratio between He^4 and H^3 is about 2, and differentiation could be made for triton energies greater than 10 Mev. The distinction between He^4 and He^3 --the ratio of ionization was about 1.5--could not usually be made. These limitations necessitated the grouping of particles into the following categories: protons, deuterons, deuterons or H^3 , H^3 or He^3 , He^3 or He^4 .

Effects of Contamination

Present in the chamber besides Xe were hydrogen and small amounts of the heavier atoms C, N, O, and Kr. In order to distinguish interactions originating in Xe from those having their origins in one of these other atoms, the observed events not associated with mesons were put into two categories. The first category included events that had more than one ionizing prong excluding the residual, while the second included events that had just one ionizing prong excluding the residual.

In treatment of events in the first category only a comparison between Xe and the heavier atoms had to be made, since two ionizing prongs could not originate from neutrons incident on hydrogen, if meson-producing collisions were neglected. Excluding H_2 , 89% by number of the atoms in the chamber were Xe. Moreover, a value for the inelastic cross section of Xe was obtained by fitting the theoretically computed formula for the cross section, using the optical model of the nucleus,⁷ to the known experimental values for neutrons near 300 Mev. From these results it was determined that only 2% of the events occurring in the heavier elements originated in C, N, O, and Kr. Consequently their presence was disregarded.

In treatment of events in the second category it was concluded that a small recoil blob would be visible at the origin of a xenon event and that this would be sufficient to distinguish it from hydrogen events. There were three reasons for this conclusion:

(a) In all but one of the 76 events in which there were two ionizing prongs, there was a characteristic recoil blob at the origin. The one exception was an event whose origin was obliterated by a background track.

(b) When all events had been identified, an investigation of those in the second category was undertaken. All those with one lightly ionizing prong and no residual had been identified as protons, in agreement with the assumption that they were hydrogen events, whereas in those events which had an associated blob 20% were identified as being something other than protons.

(c) It is known experimentally that heavy fragments produce intense ionization^{8,9} when their initial velocities fall in the range $v_0/20 < v < v_0$, where v represents the velocity of the fragment and v_0 represents the velocity of the electron in the Bohr orbit. This ionization occurs not only along the path of the fragment but also for some distance perpendicular to the path. By comparison of this experiment with a similar one using O_2 ,⁴ it was determined that the residuals of Xe events had velocities in this range. The results from O_2 indicated that every event had an associated residual blob and that the ranges of these residuals were greater than or equal to 1 mm. From published range-energy curves the energy corresponding to this minimum range was determined. Since the momentum transferred to a xenon nucleus by an incident neutron is at least equal to that transferred to an oxygen nucleus, a lower limit can be put on the velocity imparted to a xenon residual. This limit is $v \approx v_0/2$, a value which falls within the range of velocities at which intense ionization occurs. This intense ionization along and perpendicular to the path of the residual was apparent in the cloud chamber because the recoils had more than twice the thickness of lightly ionizing tracks.

Effects of contamination in meson events were negligible. No mesons were produced in the hydrogen in the chamber, since all but one meson had a residual. The one event not having a residual had an associated deuteron. Estimates based on Gasirowicz's model,¹⁰ together with available experimental information,^{3, 11} indicated that elements heavier than H_2 contributed no more than 2% to the total number of mesons observed.

III. RESULTS AND DISCUSSION

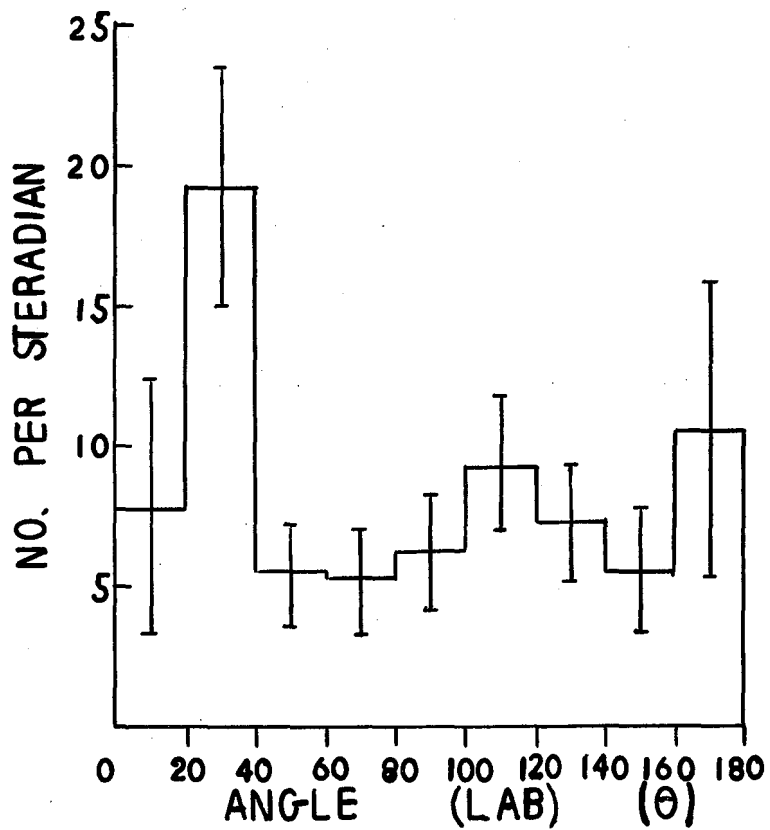
Meson Events

Angular Distribution of Mesons

The angular distribution of the mesons originating in Xe (Fig. 5) is considerably different from that obtained for the light elements. Figure 6 gives the distribution of the mesons from deuterium.¹ The average energy of the neutrons in both experiments is the same. The two plots have been normalized to give equal yields at 70° in the laboratory system. One striking difference is that the number of mesons observed per interval of solid angle between 0° and 20° for deuterium is a maximum, and a similar peaking in the forward direction was obtained for the light elements He and O_2 . For Xe there are fewer mesons per interval of solid angle between 0° and 20° than there are between 20° and 40° . Also there is a larger number of mesons emitted in the backward direction (angles greater than 90° with respect to the incident neutron direction) for Xe. The ratio of the number of mesons emitted between 0° and 90° to the number emitted between 90° and 180° is 3.8 for deuterium, while for xenon it is only 1.2.

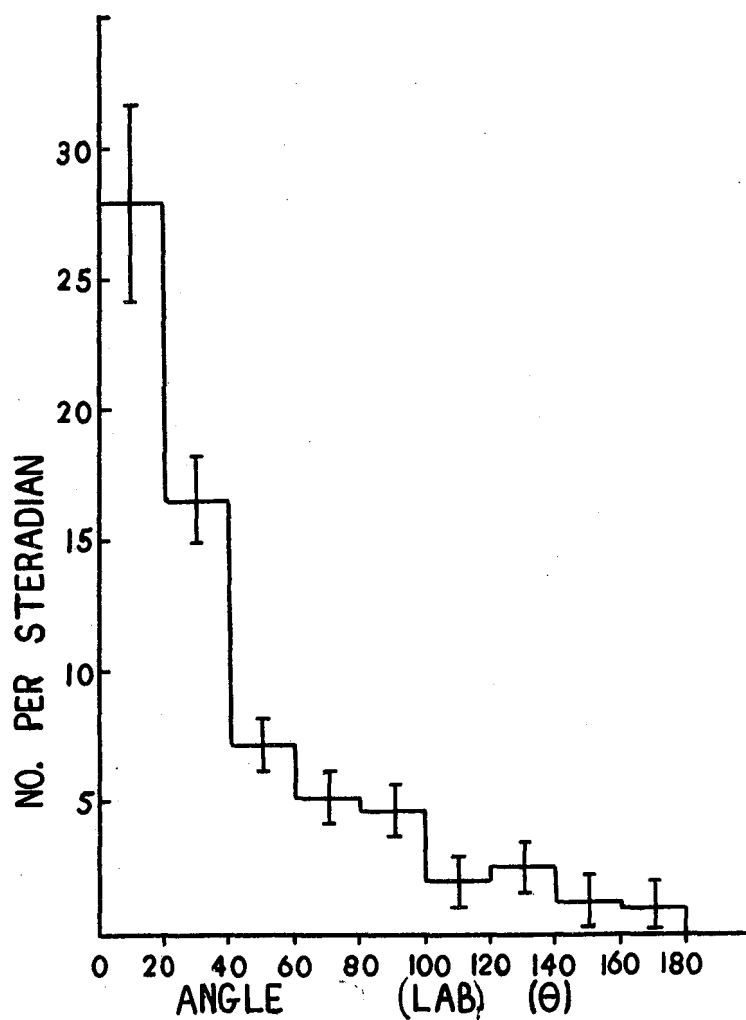
The existing experimental information on the absorption and scattering of low-energy mesons affords an explanation of the differences observed above. First, Stephen Gasirowicz¹⁰ has pointed out that the energy degradation of nucleons on first entering a nucleus decreases the volume of the nucleus in which meson production can occur. Moreover, mesons emitted at small angles to the direction of the incident nucleon have a higher energy and consequently a larger cross section for interaction with the surrounding nuclear matter. There is also ample evidence¹²⁻¹⁸ confirming the assumption that much of this interaction is associated with wide-angle scattering of the meson.

A quantitative estimate of the angular distribution of mesons emitted from heavy elements was made on the basis of a simple model (Appendix I). The energy degradation of the incident neutrons was treated in a manner similar to that used by Gasirowicz in his discussion of the energy loss of protons in heavy nuclei. A distance d was chosen such that more



MU-12364

Fig. 5. The angular distribution in the laboratory system of mesons emitted from xenon.



MU-12365

Fig. 6. The angular distribution in the laboratory system of mesons emitted from deuterium.

than 60% of the incident neutrons would suffer an energy loss by collision with a nucleon on traversing this distance within the nucleus. On the average the neutrons would lose approximately half of their energy in such a collision. Since the cross section for production of mesons drops so rapidly with decreasing energy near threshold, a small loss of energy in such a collision would essentially render the neutron incapable of producing a meson outside the volume defined by this distance d . For the neutron energy used in this experiment with volume of this zone was approximately 0.4 the volume of the nucleus. A meson produced at a point within this zone would then have to travel a certain distance through the nucleus before emerging. The probability of its being emitted from the nucleus is dependent upon whether this distance is greater or less than the mean free path for interaction of the meson.

For simplicity the following criterion was established to determine whether a meson would be absorbed before leaving the nucleus. All those mesons produced at a given point within the zone and at a given angle θ with respect to the incident neutron direction would lie along the lateral surface of a cone (Fig. A. Appendix I). To define those mesons getting out of the nucleus, a cone was chosen such that the length l of one of its elements was short enough so that more than 50% of the mesons traversing the distance l would not have suffered a collision. It was further assumed that if more than half of the circumference of the circle at the base of this cone were contained within the nucleus the mesons would not be emitted, while if more than half of the circumference were outside the nucleus the mesons would not interact before leaving the nucleus.

From the assumptions given above the effective volume of the nucleus available for meson production at a definite angle was computed (Appendix I). This volume was found to be a function of the mean free path for interaction of the incident neutron, the angle of the emitted meson, and the mean free path for interaction of the meson. The mean free path for the incident neutron, λ_n , was calculated and compared with experiment⁷ as shown in the appendix (Appendix I, Eq. (A-1)).

The mean free path of the meson, λ_a , was assumed to have an energy dependence as given by D. Stork.^{19a} The value of λ_a given by Stork includes both absorption and scattering effects, but since the scattering is largely at wide angles in the energy region considered in this experiment it was decided that both effects should be included when the mesons being scattered out of the forward direction were investigated. It was found that the values of λ_a given by partial-wave analysis (Fig. 11 of Ref. 19) gave the best fit to experimental results. Since the value of λ_a is strongly dependent upon the energy of the emitted mesons, the energy of the mesons produced at a definite angle was needed. This information was obtained from the data of M. Knapp,¹ who investigated the angular distribution of mesons emitted from deuterium with a neutron beam of the same energy. The average energy of the mesons emitted per angular interval from deuterium is given in Table I and Fig. 7 illustrates the similarity between the average energy of the mesons emitted from Xe and those from deuterium at small angles.

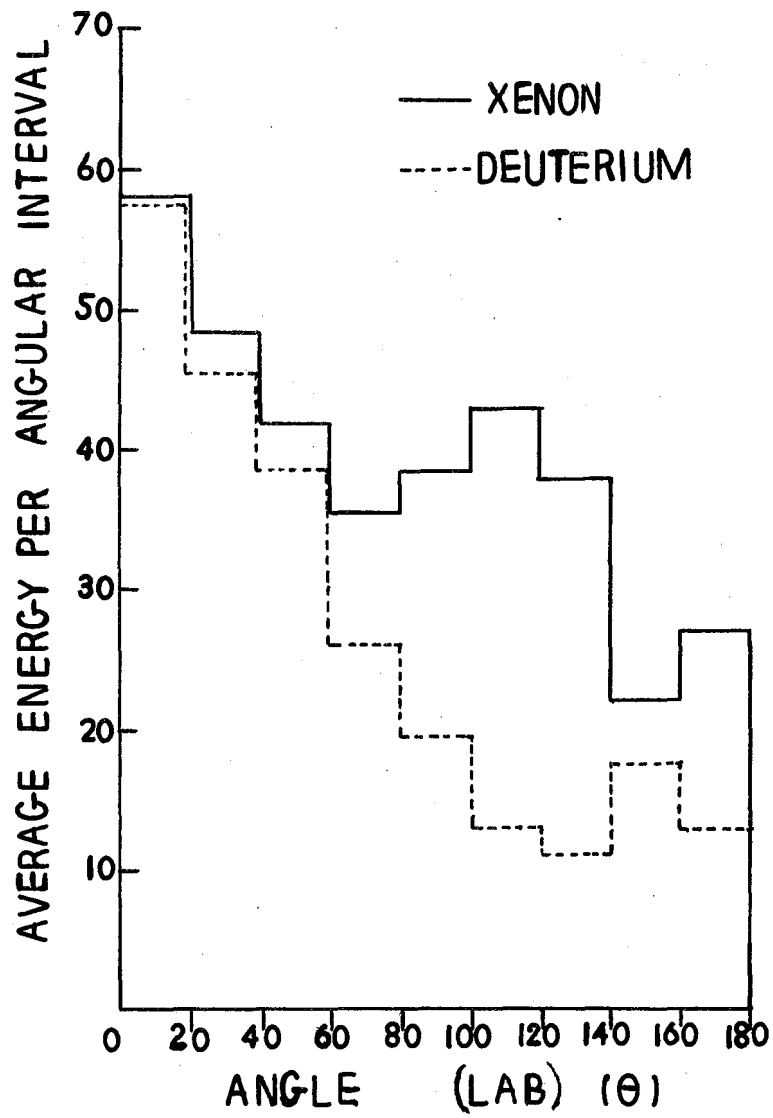
The ratio of the volume available for meson production at an angle θ to the total volume of the zone was computed for those mesons emitted at angles of 10° , 30° , and 50° . This ratio was found to be 0.40 for mesons emitted at 10° , and 0.92 for those emitted at 30° . The ratio for angles greater than or equal to 50° was unity. Figure 8 is a plot of the angular distribution of mesons from deuterium for 20° intervals after multiplication of the original distribution (Fig. 6) by the ratios stated above. Figure 5 gives the angular distribution of mesons as observed in this experiment. It would appear from comparison of the above figures that heavy nuclei are essentially transparent to the low-energy mesons emitted at larger angles to the beam, whereas they interact strongly with the higher-energy mesons emitted in the forward direction. Other experimental evidence substantiates this result.^{19, 20, 21}

Although the model used above is oversimplified, the results obtained indicate that the difference in angular distribution of the mesons emitted from Xe and those emitted from such light elements

Table I

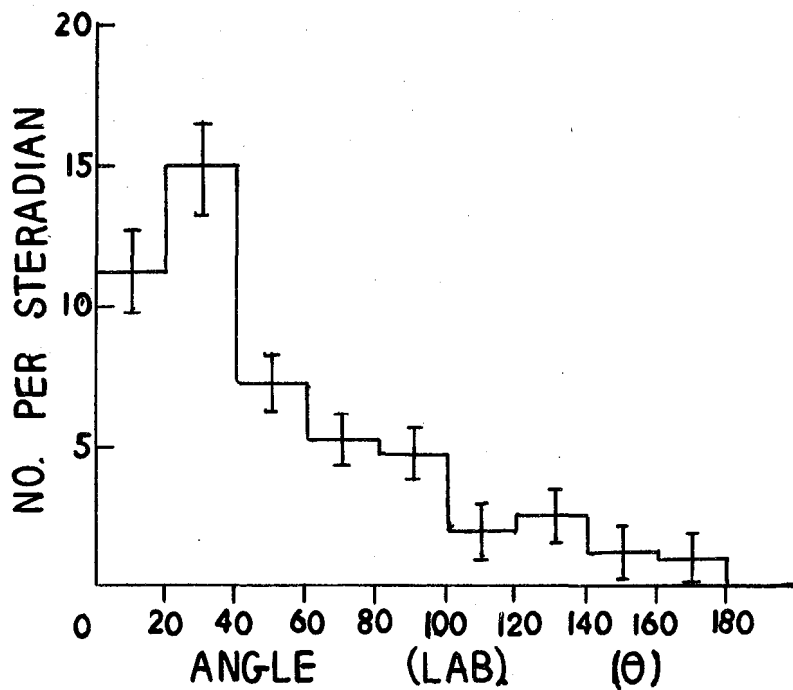
Angular distribution and average energy of mesons emitted from deuterium in the laboratory system. (Normalized at 70° to give a yield equal to that of mesons emitted from xenon at 70°)

Angular interval (degrees)	Solid angle (steradians)	Weighted no. per steradian	Average energy (Mev)
0 - 20	0.3789	28.0 ± 3.8	57.5
20 - 40	1.091	16.6 ± 1.7	45.5
40 - 60	1.672	7.3 ± 0.9	38.6
60 - 80	2.050	5.2 ± 0.7	26.1
80 - 100	2.182	4.7 ± 0.7	19.5
100 - 120	2.050	2.0 ± 0.4	12.9
120 - 140	1.672	2.6 ± 0.5	11.2
140 - 160	1.091	1.2 ± 0.5	17.3
160 - 180	0.3789	1.0 ± 0.7	12.8



MU-12366

Fig. 7. The average energy per angular interval emitted from xenon and deuterium.



MU-12367

Fig. 8. The angular distribution (in the laboratory system) of mesons emitted from deuterium after multiplication of the original distribution (Fig. 5) by the ratios discussed on page 24

as deuterium can be explained by assuming an energy degradation of the incident nucleon together with a strong energy dependence for the interaction mean free path of the mesons produced within the nucleus. The greater number of mesons scattered at large angles for Xe is consistent with the fact that part of the interaction of the meson and the nucleons in the nucleus results in wide-angle scattering.

Energy Distribution of Mesons

The energy distribution of the mesons in the laboratory system is given in Table II and plotted in Fig. 9. Included for comparison is a plot of the meson-energy spectrum from deuterium. The deuterium curve has been altered to give a yield of mesons at 70 Mev (60 to 80) equal to that of the mesons from Xe at 70 Mev.

Within the statistical limits of the experiments the shapes of the two curves are quite similar, even at the higher energies. The meson-energy spectrum from oxygen,³ when compared with that from Xe, also agreed throughout the energy range. This similarity is not inconsistent with the larger cross section for interaction of mesons at higher energies, since most of the interaction with the heavy nuclei consists of scattering through large angles, as opposed to complete absorption.²²

Plotted in Fig. 7 are the average energies of the mesons emitted from xenon and deuterium per 20° interval in the laboratory system. The standard deviations for xenon are given in Table III. Although the two curves are quite similar at the smaller angles, the decrease of energy with angle is considerably less for xenon than for deuterium.

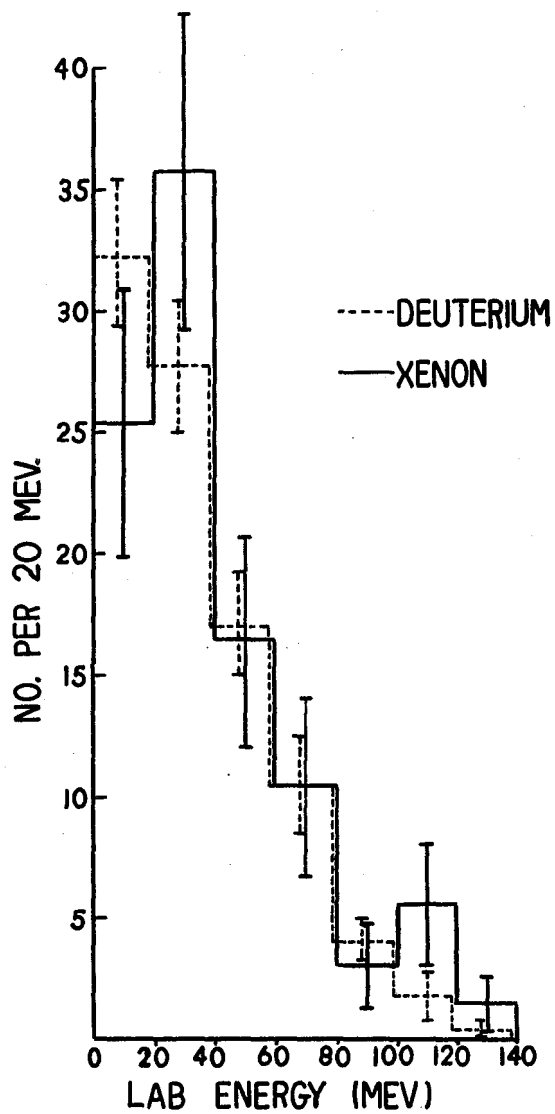
Energy of Neutrons Producing Mesons

The energy of the neutron producing each meson could be determined for the light elements by balancing momentum and energy for each event. Such a procedure was found to be unreliable for the meson events in Xe. The residuals in most cases were too short in range and too poorly defined in direction to permit a determination of either their

Table II

Xenon pion energy spectrum

Energy range (Mev)	Total number	Weighted number
0 - 20	22	25.4 ± 5.5
20 - 40	32	35.8 ± 6.5
40 - 60	15	16.4 ± 4.3
60 - 80	9	10.4 ± 3.7
80 -100	3	3.0 ± 1.7
100 -120	5	5.5 ± 2.5
120 -140	1	1.4 ± 1.4



MU-12368

Fig. 9. The energy distribution (in the laboratory system) of mesons emitted from xenon and deuterium.

Table III

Angular distribution of mesons emitted from xenon
in the laboratory system

Angular interval (degrees)	Total number	Weighted Number	Solid angle (steradians)	Weighted no. per steradian	Average energy (Mev)
0 - 20	3	3.0 ± 1.7	0.3789	7.9 ± 4.6	58.1 ± 4.6
20 - 40	21	21.0 ± 4.6	1.091	19.3 ± 4.2	48.3 ± 7.1
40 - 60	9	9.0 ± 3.0	1.672	5.4 ± 1.8	41.9 ± 9.3
60 - 80	8	10.6 ± 3.8	2.050	5.2 ± 1.8	35.5 ± 6.3
80 -100	9	13.4 ± 4.5	2.182	6.2 ± 2.0	38.5 ± 8.0
100 -120	15	19.2 ± 5.0	2.050	9.4 ± 2.4	43.0 ± 11.0
120 -140	12	12.0 ± 3.5	1.672	7.2 ± 2.1	37.8 ± 7.2
140 -160	6	6.0 ± 2.5	1.091	5.5 ± 2.3	22.0 ± 5.7
160 -180	4	4.0 ± 2.0	0.3789	10.6 ± 5.3	26.8 ± 4.4

energy or momentum. In addition, the increased Coulomb barrier caused a decrease in the number of charged particles associated with mesons from Xe. Consequently only six events were found that could be balanced with any certainty.

The energy spectra of the neutrons producing mesons in deuterium¹ and He² are plotted in Fig. 10, and are assumed to be good representations of the energy spectrum of the neutrons producing mesons in Xe. The above assumption is based on the following considerations. Firstly, the energy of the incident neutron beam was quite similar in the three experiments (Fig. 1). Secondly, the plots in Fig. 10 illustrate the similarity of the neutron spectrum producing mesons in deuterium to that producing mesons in He. Finally, the momentum distribution of the nucleons in the nucleus does not change appreciably with increasing atomic weight for elements heavier than deuterium.²³

Classification and Analysis of Prongs Associated with Mesons

Information concerning the types of meson events observed is contained in Table IV. Energy and angular distributions for the protons associated with meson events are given in Tables V, VI, and VII, and plotted in Figs. 11 and 12. Included for comparison is the same information for the protons associated with meson events as observed in deuterium.

Analysis of the above information illustrates the effect of the increased Coulomb barrier for heavy elements. In a similar experiment, performed with O₂ as the target element, Ford³ found that meson events with four or more associated prongs constituted approximately four-tenths of the total number of meson events observed. In Xe, however, only two of the 87 events have four associated prongs, and no events of higher multiplicity were observed. In addition a type of meson event not observed by Ford was discovered in the Xe experiment. Fifteen of the meson events in Xe consisted of only the meson and a short residual, with no other associated prongs. (Fig. 13). A likely interpretation of this type of event would

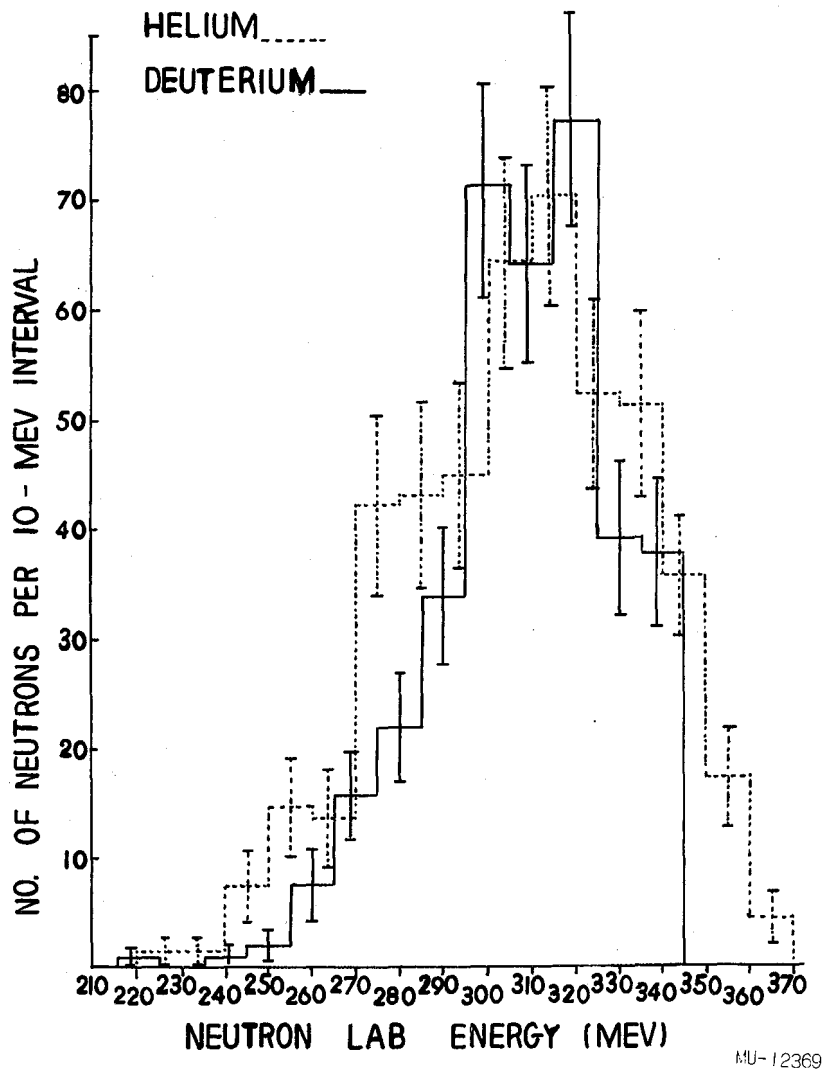


Fig. 10. The energy spectrum of those neutrons producing mesons in helium and deuterium.

Table IV

Prongs associated with negative meson production in xenon						
Identification of events ^a	Number observed	Most energetic prong, as indicated				
		Proton	Deuteron	H ² or H ³	HE ³ or $\overline{\text{H}}^3$	or UNC.
(π^- , R)	15	---	-	-	-	-
(π^- , d, R)	11	---	11	-	-	-
(π^- , d or t, R)	10	---	9	10	-	-
(π^- , p, R)	30	30	-	-	-	-
(π^- , U, R)	2	---	-	-	-	2
(π^- p, d, R)	2	2	-	-	-	-
(π^- , p, d or t, R)	4	1	2	3	-	-
(π^- , p, U, R)	3	---	-	-	-	3
(π^- , p, p, R)	5	5	-	-	-	-
(π^- , p, t or HE ³ , R)	2	---	-	2	2	-
(π^- , t, d or t, R)	1	-	1	1	-	-
(π^- , p, p, U, R)	1	-	-	-	-	1
(π^- , p, d, U, R)	1	-	-	-	-	1
Total	87	38	11	14	2	7

^a Identification key:
 U represents unidentified prongs.
 R represents the residuals.

Table V

Energy distribution (in the laboratory system) of protons associated with mesons emitted from xenon and deuterium

Xenon		Energy range (Mev)	Deuterium	
Total number	Weighted number		Total number	Weighted number
10	12.4 ± 4.0	0 - 10	143	173.2 ± 13.2
11	14.6 ± 4.5	10 - 20	37	44.3 ± 6.5
4	5.7 ± 2.9	20 - 30	35	42.7 ± 6.5
6	6.6 ± 2.7	30 - 40	24	26.7 ± 5.1
7	8.1 ± 3.1	40 - 50	25	27.9 ± 5.1
3	3.5 ± 2.1	50 - 60	20	24.5 ± 5.2
6	8.0 ± 2.6	60 - 70	13	14.9 ± 4.1
1	1.0 ± 1.0	70 - 80	13	17.0 ± 4.3
2	2.0 ± 1.4	80 - 90	14	16.1 ± 4.2
1	1.0 ± 1.0	90 - 100	21	25.4 ± 5.4
2	2.5 ± 1.8	100 - 110	13	18.1 ± 4.5
0	0.0	110 - 120	13	14.9 ± 4.0
1	1.5 ± 1.5	120 - 130	1	1.0 ± 1.0
0	0.0	130 - 140	5	5.5 ± 2.4
0	0.0	140 - 150	2	2.7 ± 1.6
0	0.0	150 - 160	4	4.3 ± 2.0

Table VI

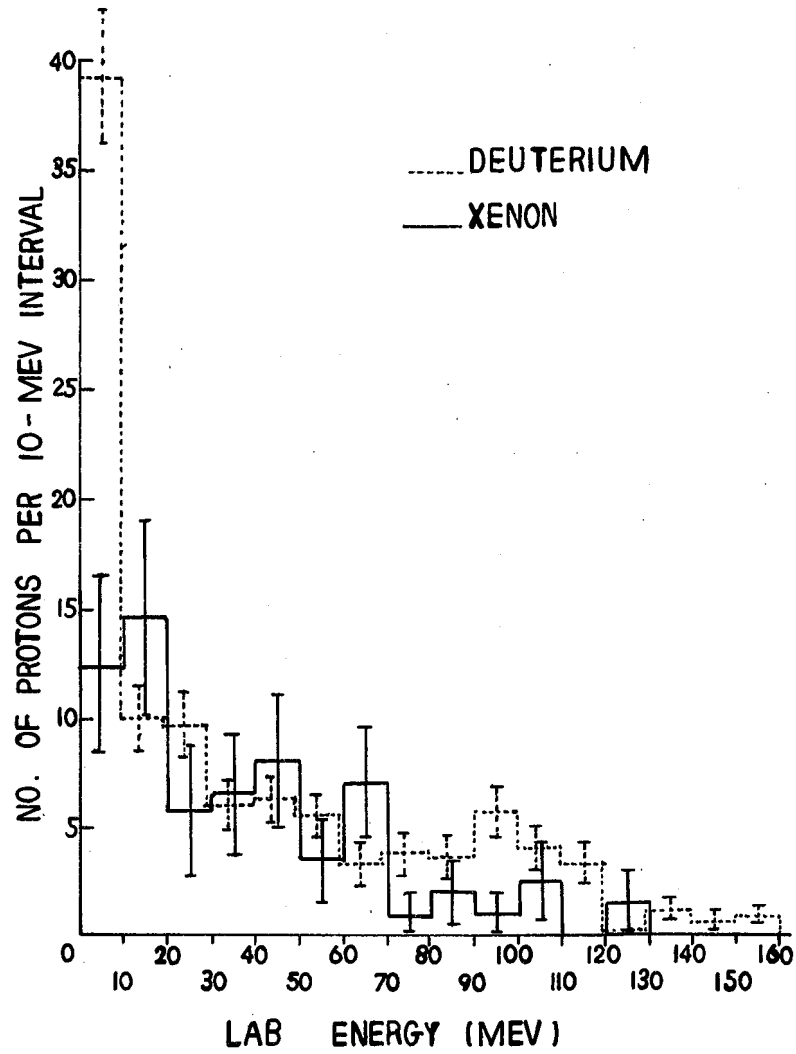
Angular distribution (in the laboratory system) of protons associated with mesons emitted from xenon

Angular interval	Total number	Weighted number	Weighted number per steradian
0 - 20	12	13.9 ± 4.1	36.8 ± 10.8
20 - 40	13	14.4 ± 4.0	13.2 ± 3.7
40 - 60	11	13.0 ± 4.0	7.8 ± 2.4
60 - 80	9	12.8 ± 4.4	6.2 ± 2.1
80 -100	3	4.7 ± 2.7	2.2 ± 1.2
100 -120	1	2.0 ± 1.4	0.98 ± 0.7
120 -140	3	3.7 ± 2.2	2.2 ± 1.3
140 -160	2	2.0 ± 1.4	1.8 ± 1.3
160 -180	0	0.0	0.0

Table VII

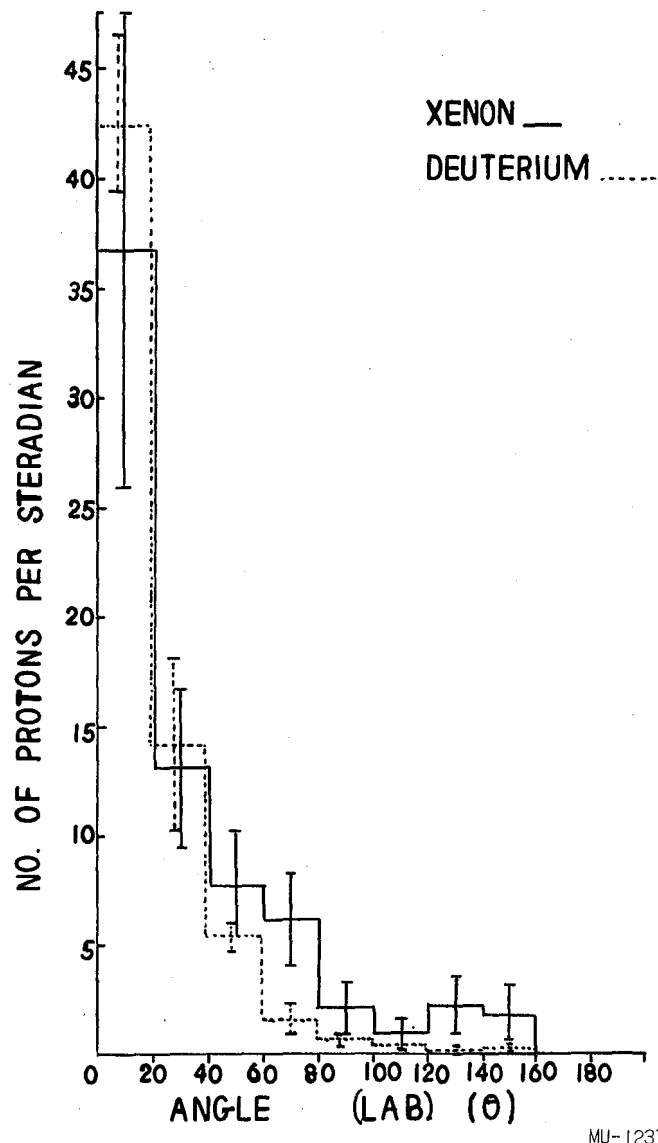
Angular distribution (in the laboratory system) of protons associated with mesons emitted from deuterium

Angular interval	Total number	Weighted number	Weighted number per steradian
0 - 20	135	154.5 ± 13.6	407.6 ± 35.9
20 - 40	118	149.2 ± 14.3	136.7 ± 37.7
40 - 60	72	86.3 ± 10.0	51.6 ± 6.0
60 - 80	25	29.9 ± 6.2	14.6 ± 3.0
80 -100	11	12.4 ± 4.9	5.7 ± 2.2
100 -120	6	7.5 ± 2.6	3.7 ± 1.3
120 -140	1	1.0 ± 1.0	0.6 ± 0.6
140 -160	1	1.0 ± 1.0	0.9 ± 0.9
160 -180	0	0.0	0.0



MU-12370

Fig. 11. The energy distribution(laboratory system)of protons associated with meson events in xenon and deuterium. Arbitrary normalization.



MU-12371

Fig. 12. The angular distribution (in the laboratory system) of protons associated with meson events in xenon and deuterium. Arbitrary normalization.



ZN-1600

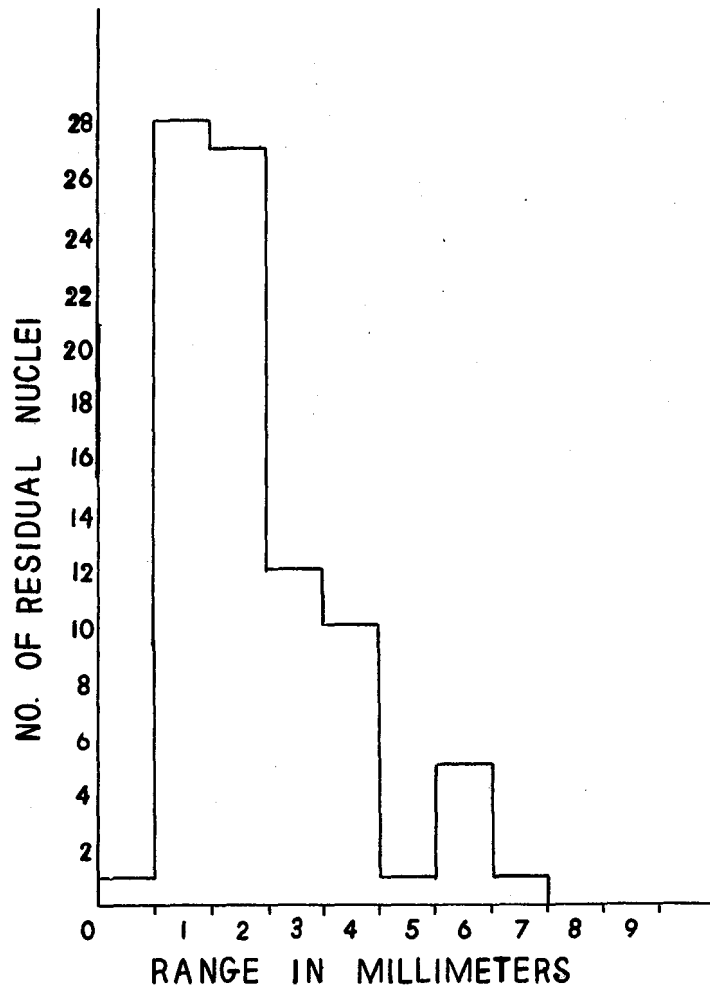
Fig. 13. A meson event occurring in Xe and consisting of a meson (1) and a residual (arrow). For other meson events occurring in Xe see Fig. B, Appendix II.

be that the proton resulting from the production of a meson when the incident neutron struck a nucleon in the nucleus had too small an energy to scale the Coulomb barrier. The plot of the proton-energy spectrum associated with meson production (Fig. 11) also illustrates this effect. There was no such large number of protons of less than 10 Mev observed with xenon as had been observed in the deuterium experiment.

The small number of events and the question concerning identification did not permit any definite comparisons for the deuterons associated with meson production. It was found, however, that the ratio of fast protons to fast deuterons in the case of xenon was equal to that for oxygen³ if those prongs classified as either deuterons or tritons were called deuterons. This would at least indicate that deuteron formation is not appreciably altered with increasing atomic weight.

Residual Nuclei

The range distribution for the short residuals associated with meson events is plotted in Fig. 14. The median range was found to be approximately 2.5 mm. The energy to be ascribed to such a range was determined in the following manner. First, those meson events which could be balanced yielded a value for the energy of the residual. A plot was made of range vs energy for these residuals and the best fit to a straight line was determined. Secondly, an independent determination was made by the use of a range-energy formula similar to that proposed by N. Bohr.⁸ This formula predicts a linear relationship between range and energy, which is in agreement with experiment.⁹ The two determinations agreed to within 20%. The energy of a xenon residual of 2.5 mm range was thus determined as approximately 4.5 Mev.



MU-12372

Fig. 14. Distribution of the ranges of the residual nuclei occurring in meson events in xenon.

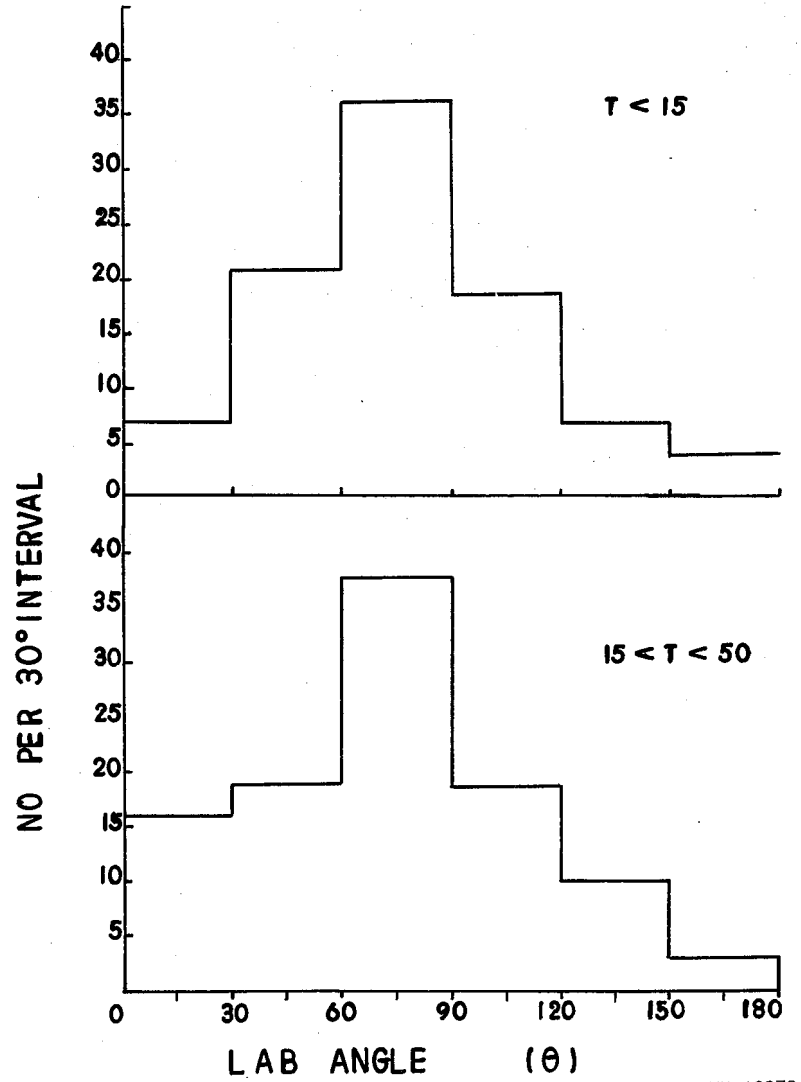
Events Not Associated with Mesons

Angular and Energy Distributions of Protons

The angular distributions of protons emitted from Xe for different energy intervals are given in Figs. 15 and 16. These figures illustrate the tendency for the higher-energy protons to be more concentrated in the forward direction. Figure 17 is a plot of the number of protons from Xe per 10^0 interval for all protons greater than 15 Mev, while Fig. 18 includes only those protons from 2-prong stars. Included for comparison in both cases is a similar plot for protons emitted from oxygen. One apparent difference between the oxygen and Xe curves in Figs. 17 and 18 is the flatter distribution of protons from Xe at smaller angles. This is in qualitative agreement with the prediction of the cascade model.²⁴ Tables VIII and IX include the angular distribution of protons from Xe per unit of solid angle, and the plot of this distribution is given in Fig. 19. The statistical errors are large at the smaller angles, but no appreciable forward dip is present. The energy distributions of protons from xenon and oxygen are given in Figs. 20 and 21. Figure 22 (a) includes all particles of charge 1 from xenon, together with the theoretical curve of LeCouteur.²⁵ In Fig. 23 the energy spectra of protons from Xe emitted in the forward and backward hemispheres are compared, and are in favorable agreement with similar curves obtained from silver by L. Bailey.²⁶

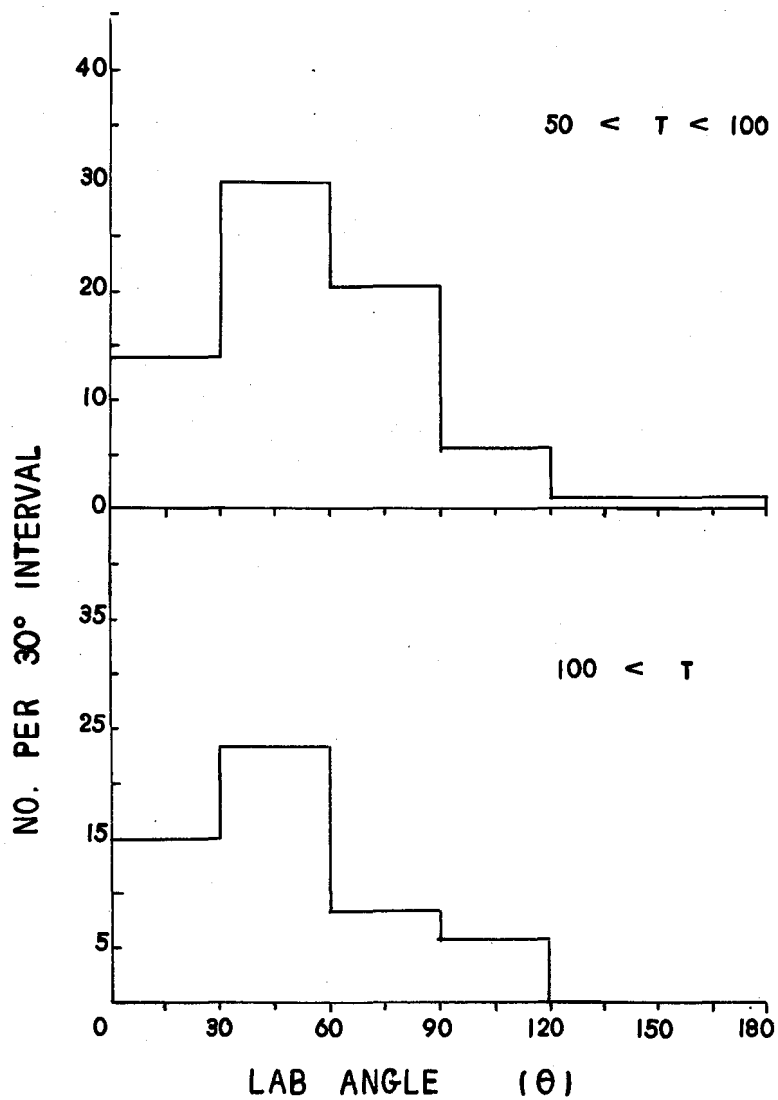
Angular and Energy Distributions of Deuterons

Because deuterons cannot be distinguished from tritons for all energy ranges, it is impossible to discuss the deuteron distributions alone. Consequently, Figs. 24, 25, and 26 contain the two classifications "deuterons" and "deuterons or tritons". The energy and angular distributions of deuterons from xenon and oxygen are in fair agreement, and the decrease of deuteron yield with increasing energy is consistent with the theory of secondary pickup.



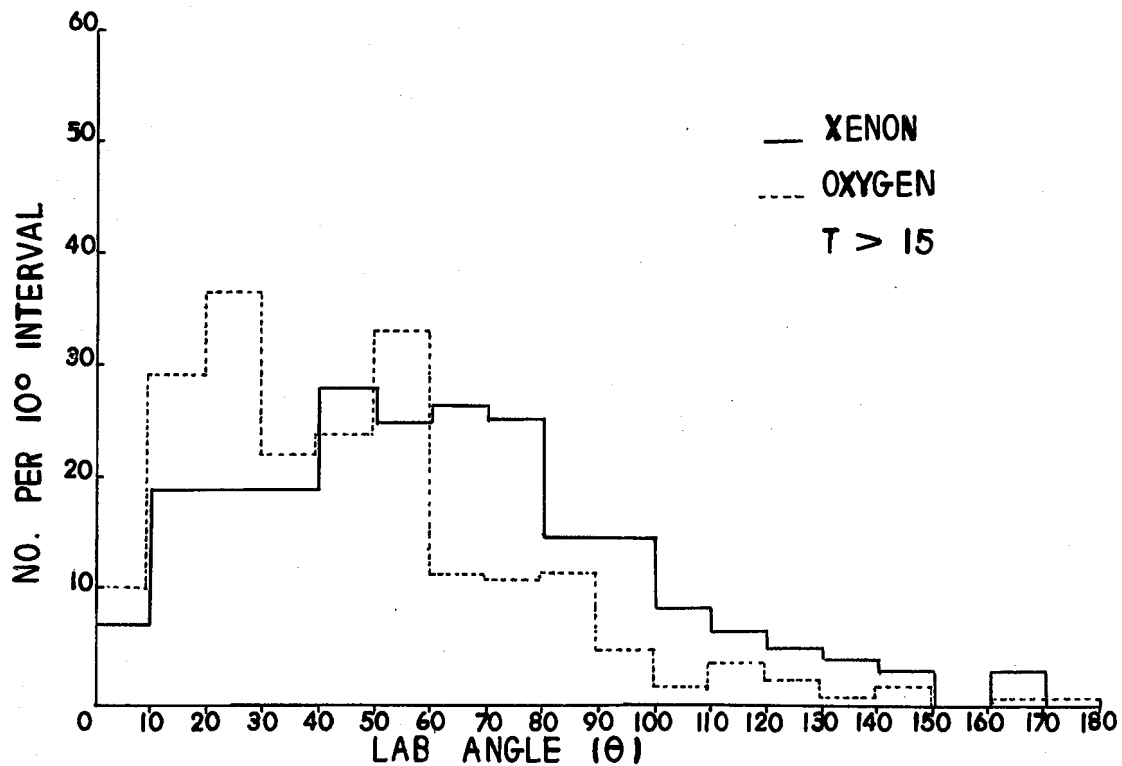
MU-12373

Fig. 15. The angular distribution (in the laboratory system) of protons emitted from xenon occurring in events not associated with mesons. Upper: the energies are less than 15 Mev. Lower: the energies of the protons are between 15 and 50 Mev.



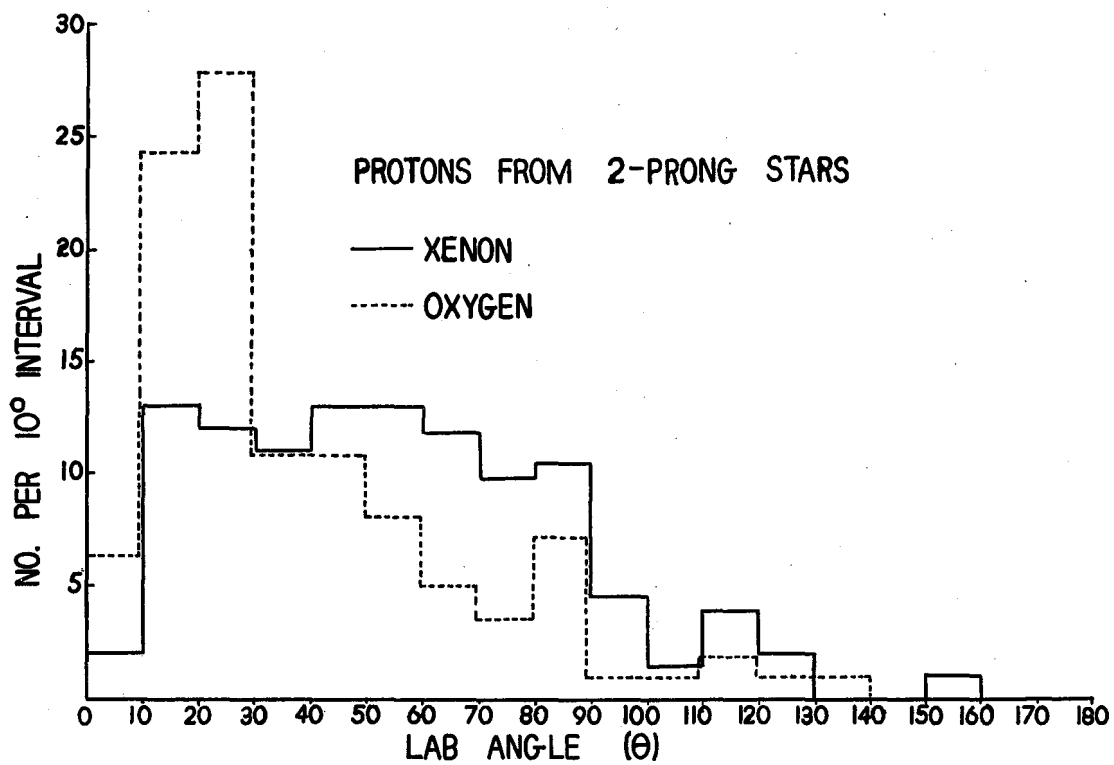
MU-12374

Fig. 16. The angular distribution (in the laboratory system) of protons emitted from xenon occurring in events not associated with mesons. Upper: the energies of the protons are between 50 and 100 Mev. Lower: energies exceed 100 Mev.



MU-12375

Fig. 17. The angular distribution (in the laboratory system) of all protons of energy greater than 15 Mev and occurring in events not associated with mesons.



MU-12376

Fig. 18. The angular distribution (in the laboratory system) of protons from 2-prong stars.

Table VIII

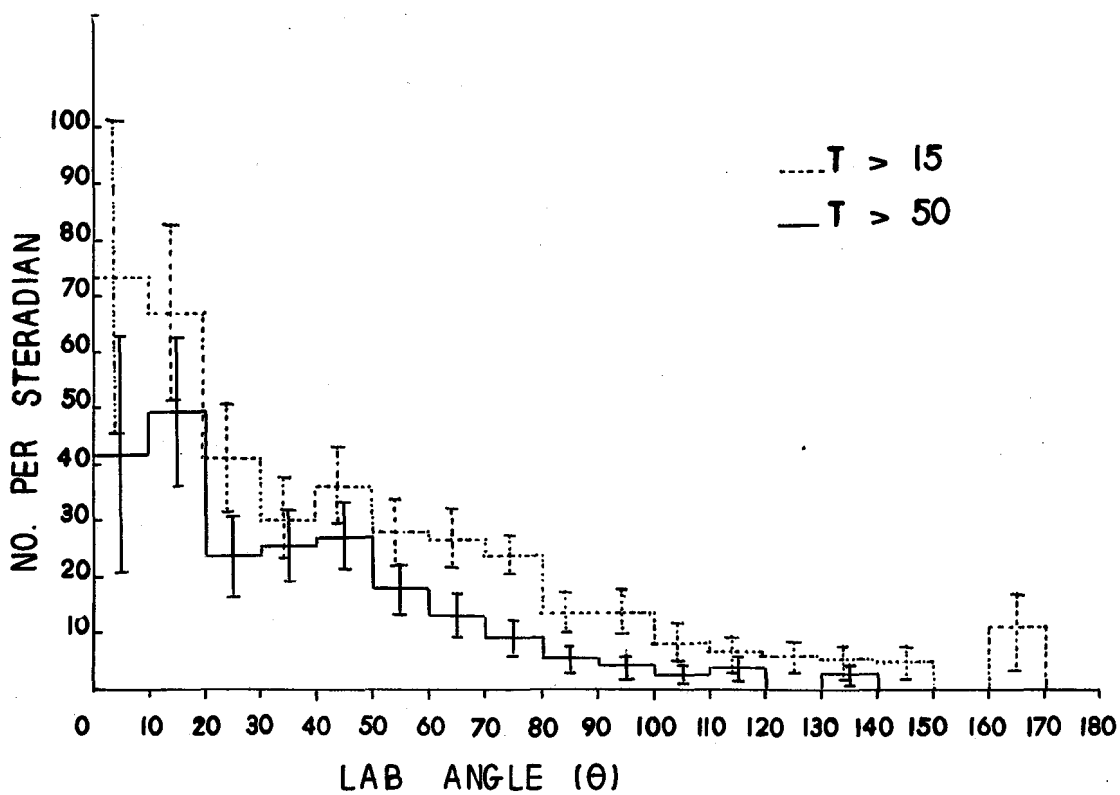
Number of protons per unit of solid angle emitted from xenon with energies exceeding 15 Mev

Angular interval	Total number	Weighted number	Solid angle (sterad)	Weighted no. per steradian
0 - 10	7.0	7.0	0.09544	73.4 ± 27.7
10 - 20	19.0	19.0	0.2835	67.0 ± 15.4
20 - 30	19.0	19.0	0.4628	41.1 ± 9.4
30 - 40	19.0	19.0	0.6283	30.2 ± 6.9
40 - 50	28.0	28.0	0.7744	36.2 ± 6.8
50 - 60	25.0	25.0	0.8972	27.8 ± 5.6
60 - 70	22.0	26.4	0.9926	26.6 ± 5.2
70 - 80	18.0	25.3	1.0579	23.9 ± 3.2
80 - 90	10.0	14.9	1.0910	13.6 ± 3.5
90 -100	10.0	14.8	1.0910	13.6 ± 3.5
100 -110	6.0	8.5	1.0579	8.05 ± 2.8
110 -120	5.0	6.5	0.9926	6.55 ± 2.6
120 -130	5.0	5.0	0.8972	5.68 ± 2.5
130 -140	4.0	4.0	0.7744	5.17 ± 2.7
140 -150	3.0	3.0	0.6283	4.78 ± 2.8
150 -160	0.0	0.0	0.4628	0.0
160 -170	3.0	3.0	0.2835	10.6 ± 6.1
170 -180	0.0	0.0	0.9544	0.0

Table IX

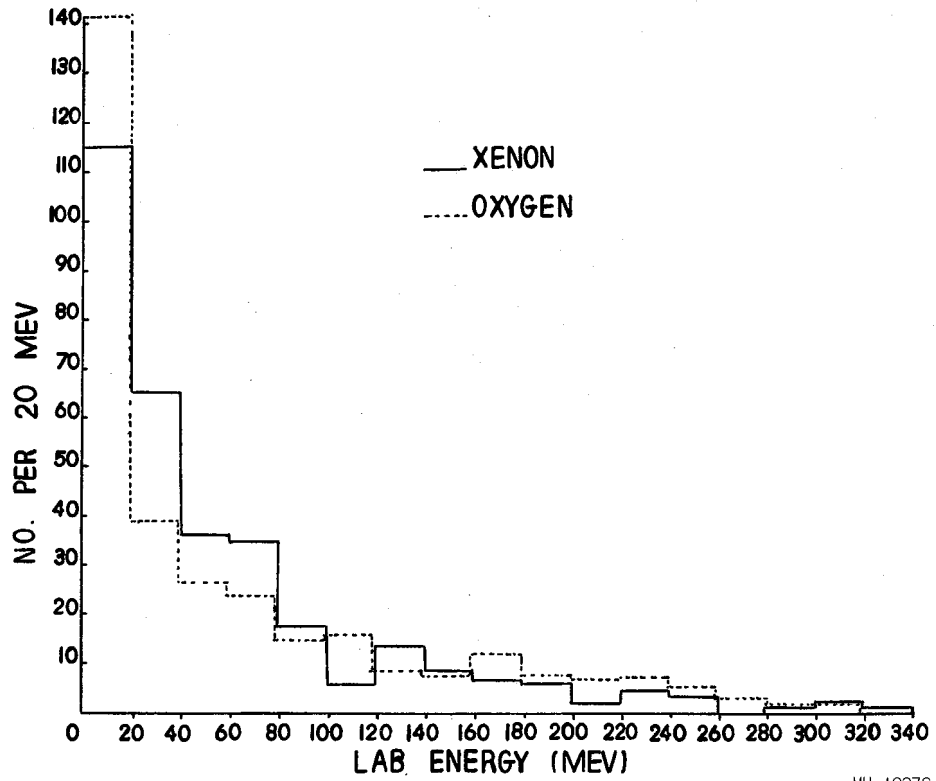
Number of protons per unit of solid angle emitted from xenon with energies exceeding 50 Mev

Angular Interval	Total number	Weighted number	Solid angle (sterad)	Weighted number per steradian
0 - 10	4.0	4.0	0.09544	41.9 ± 21.0
10 - 20	14.0	14.0	0.2835	49.4 ± 13.2
20 - 30	11.0	11.0	0.4628	23.8 ± 7.2
30 - 40	16.0	16.0	0.6283	25.5 ± 6.4
40 - 50	21.0	21.0	0.7744	27.1 ± 5.9
50 - 60	16.0	16.0	0.8972	17.8 ± 4.5
60 - 70	11.0	13.1	0.9926	13.2 ± 3.8
70 - 80	7.0	9.8	1.0579	9.28 ± 3.0
80 - 90	4.0	5.94	1.0910	5.44 ± 2.2
90 -100	3.0	4.47	1.0910	4.1 ± 1.9
100 -110	2.0	2.8	1.0579	2.65 ± 1.6
110 -120	3.0	3.9	0.9926	3.93 ± 2.0
120 -130	0.0	0.0	0.8972	0.0
130 -140	2.0	2.0	0.7744	2.58 ± 1.8
140 -150	0.0	0.0		0.0
150 -160	0.0	0.0		0.0
160 -170	0.0	0.0		0.0
170 -180	0.0	0.0		0.0



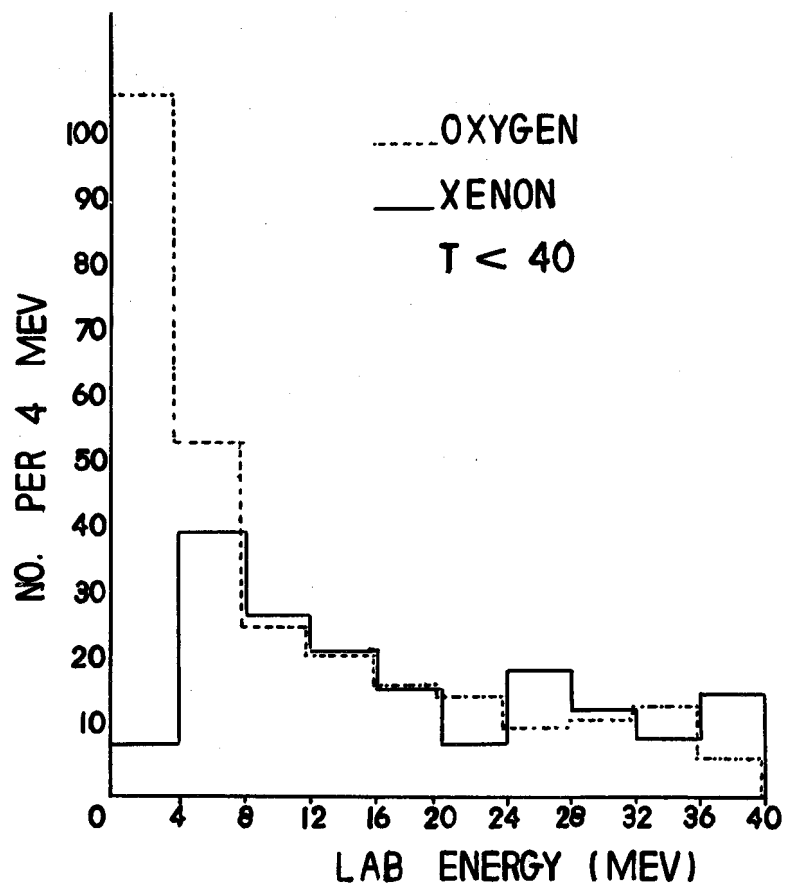
MU-12377

Fig. 19. Angular distribution (in the laboratory system) of protons per unit of solid angle. The continuous plot includes all protons with energies greater than 50 Mev; the dotted plot includes protons with energies greater than 15 Mev.



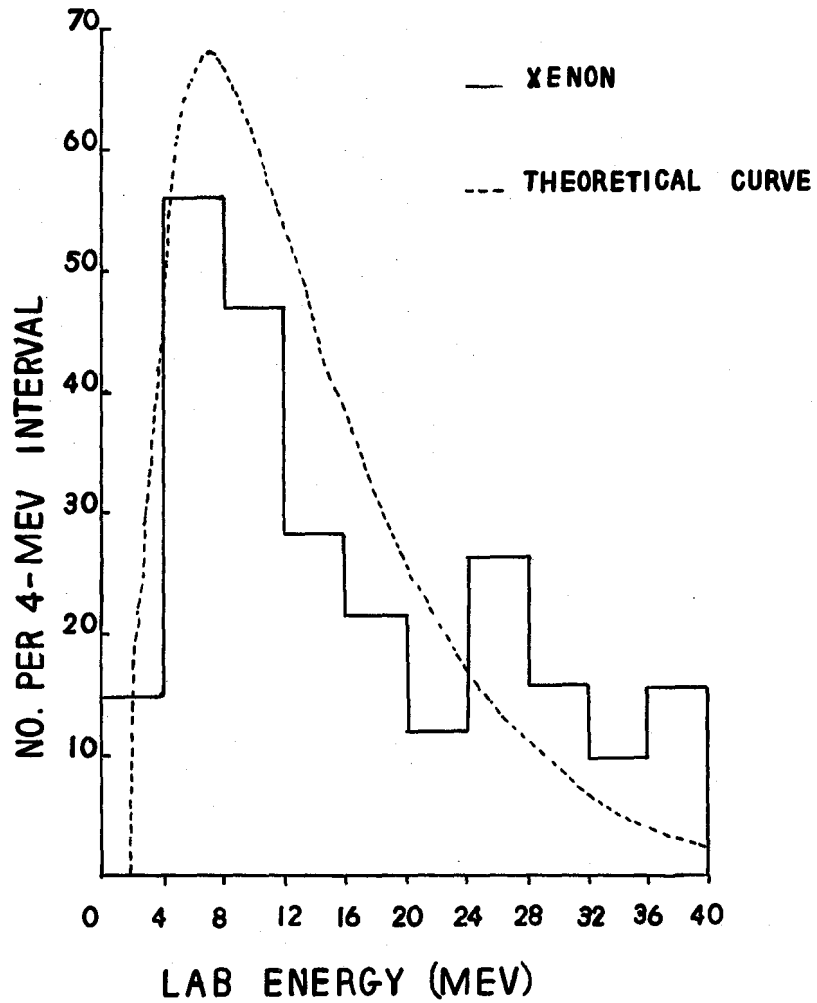
MU-12378

Fig. 20: The energy distribution (in the laboratory system) of all protons.



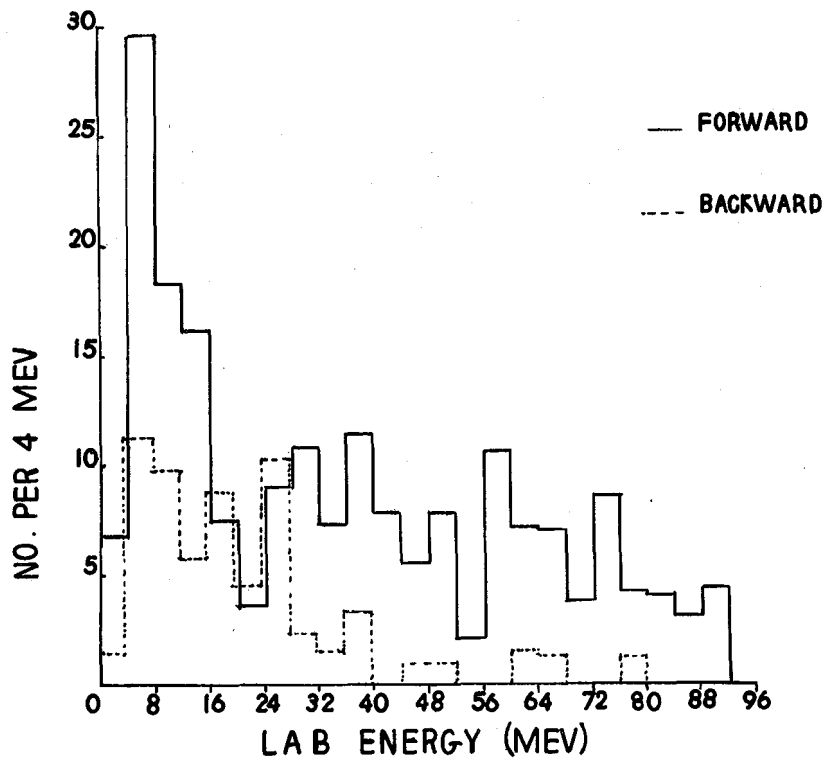
MU-12379

Fig. 21. The energy distribution (in the laboratory system) of protons with energies less than 40 Mev.



MU-12380

Fig. 22. The energy spectrum of all particles of unit charge emitted from Xe. The curve represented by the broken line is the theoretical curve of LeCouteur, which includes the effect of the decreased Coulomb barrier due to excitation of the nucleus.



MU-12381

Fig. 23. The energy spectrum of protons emitted from Xe in the energy interval 0-92 Mev. The protons have been divided into two groups, those emitted in the forward hemisphere (solid line) and those emitted in the backward hemisphere (broken line).

Heavier Particles

Classification of particles heavier than deuterons is included in Table X. The small number of such particles observed and the uncertainty of identification does not permit any comparisons to be made.

Residual Nuclei

Ranges of residuals for events not associated with mesons are plotted in Fig. 27. The median range corresponds to an energy of approximately 2 Mev.

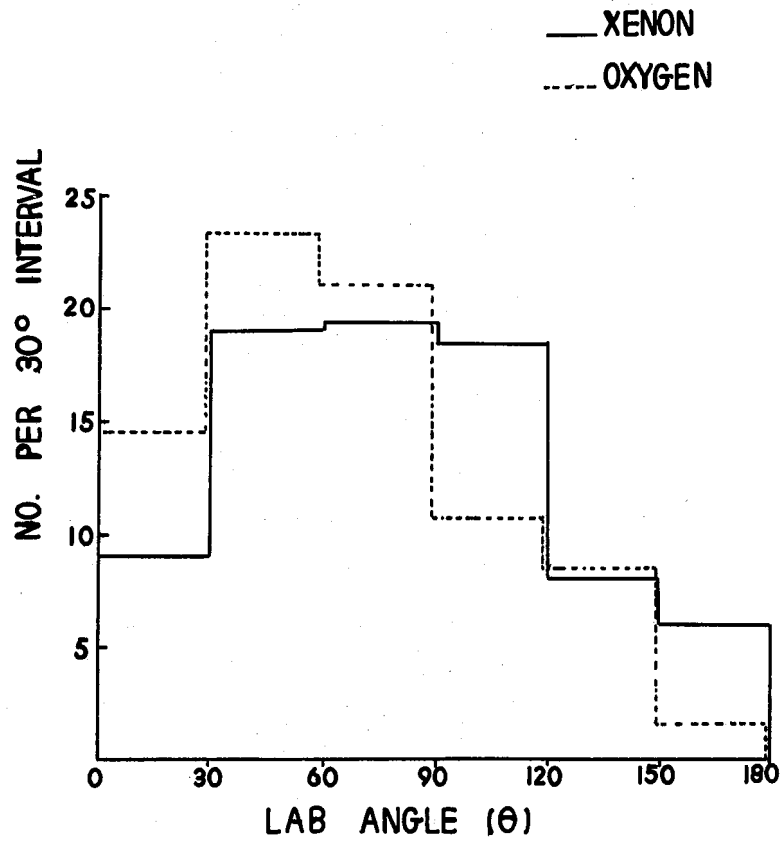
Star Yield Versus Neutron Energy

In order to determine the percentage yield of stars from xenon for different portions of the neutron energy spectrum, a method similar to that discussed by M. Fuller⁴ was adopted. A plot of the neutron energy spectrum as obtained by W. Ball,²⁷ extended to lower energies, is illustrated in Fig. 28. Included is a histogram of the neutron-energy spectrum as obtained in this experiment. The inelastic cross section of xenon was determined at 280 Mev and at 90 Mev from S. Fernbach,⁷ and at 10 Mev from H. Feshbach and V. Weisskopf.²⁸ The resulting yields are:

Percentage of total stars	Neutron energy
57%	$280 < T$
19%	$200 < T < 280$
12%	$100 < T < 200$
4%	$60 < T < 100$
8%	$0 < T < 60$

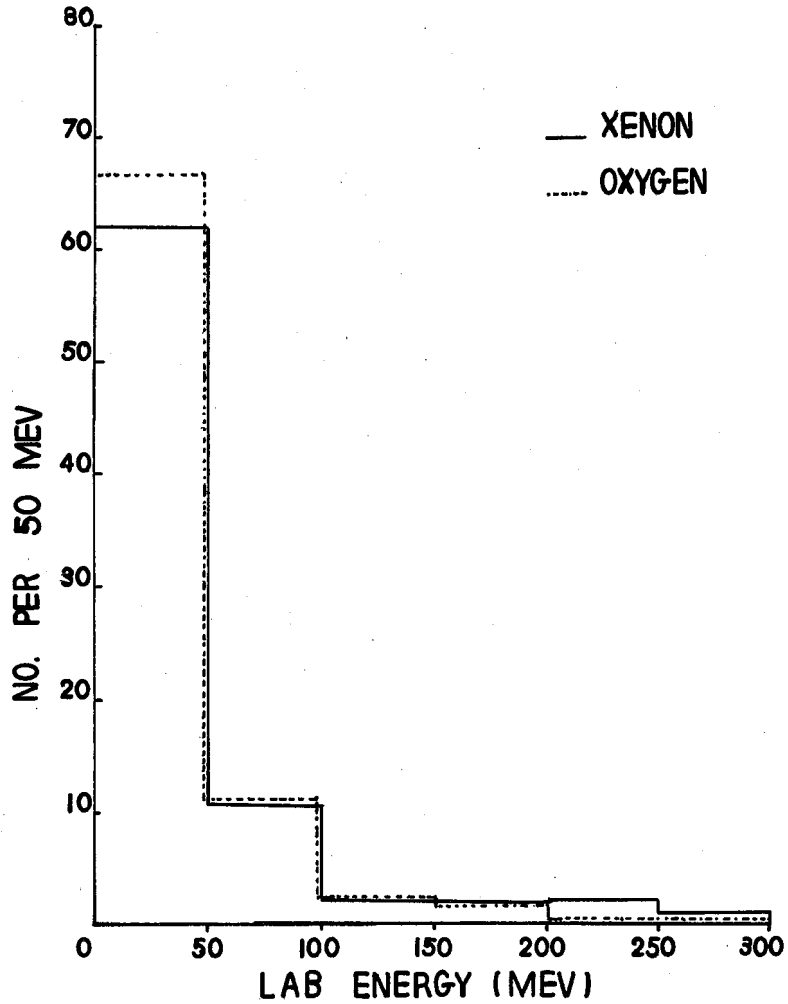
Azimuthal Symmetry Check

In the analysis of events, prongs with dip angles greater than 60° were counted but were not included in the various distributions presented here. Their absence has been accounted for by a statistical weighting factor³ based on the assumption of azimuthal symmetry.



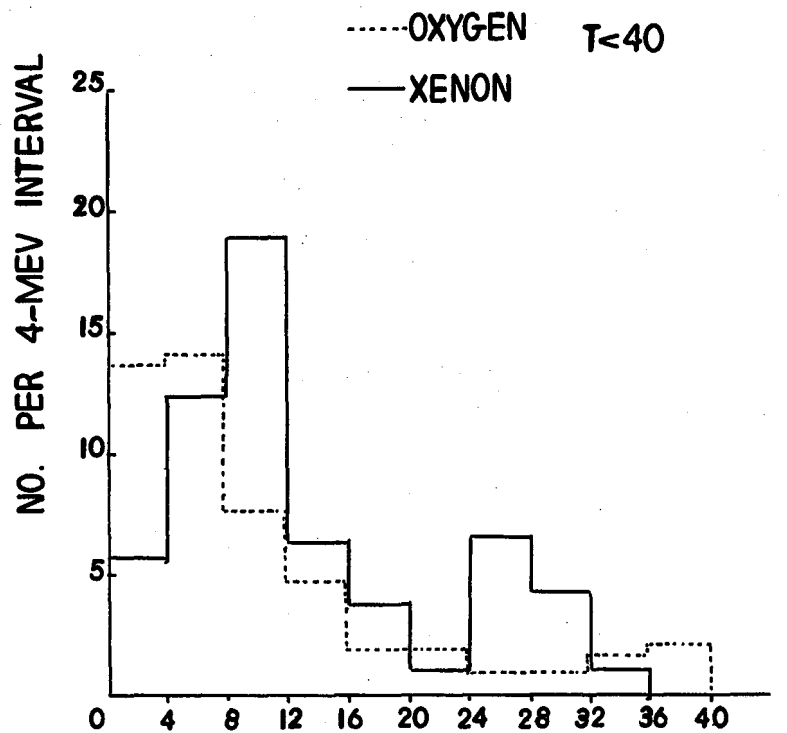
MU-12382

Fig. 24. The angular distribution (in the laboratory system) of deuterons and "deuterons or tritons" occurring in events not associated with mesons.



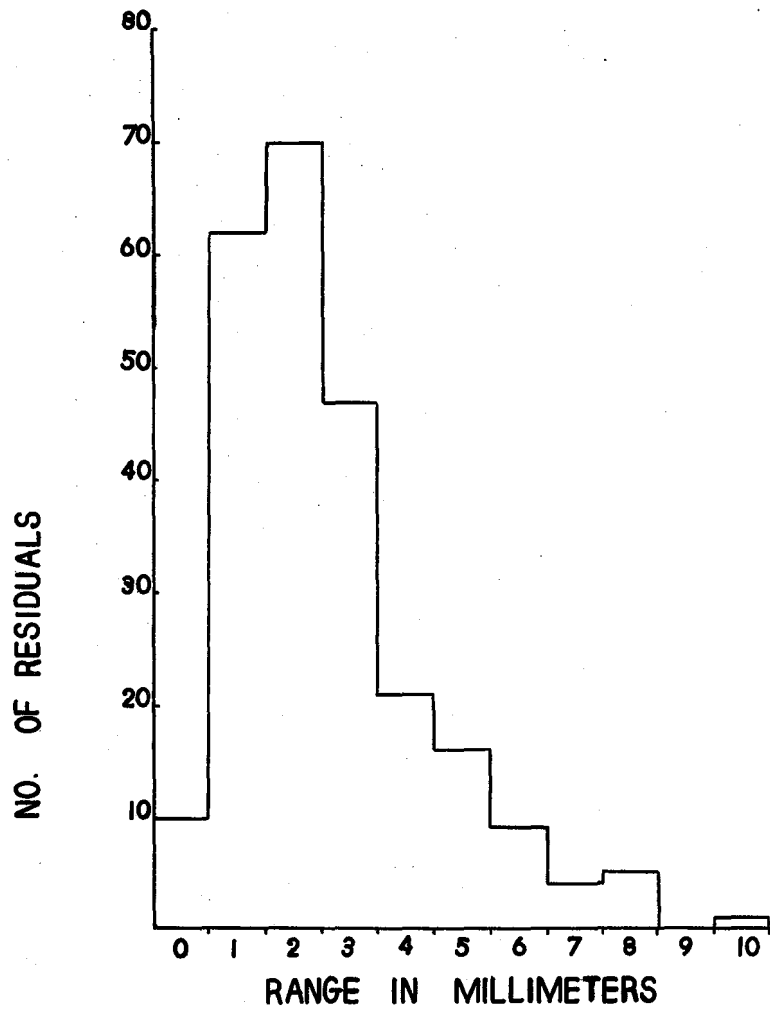
MU-12383

Fig. 25. The energy distribution (in the laboratory system) of deuterons and "deuterons or tritons" occurring in events not associated with mesons.



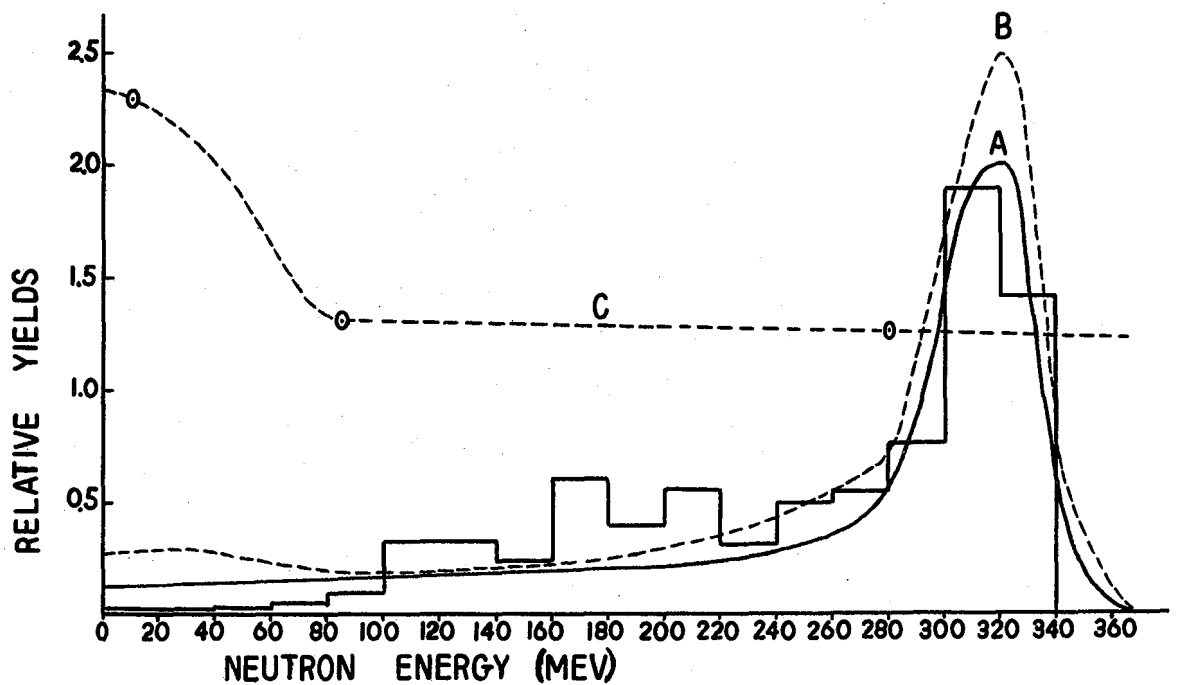
MU-12384

Fig. 26. The energy distribution (in the laboratory system) of deuterons and "deuterons and tritons" with energies less than 40 Mev.



MU-12385

Fig. 27. Distribution of the ranges of the residual nuclei occurring in nonmeson events in xenon.



MU-12386

Fig. 28. Curve A is W. Ball's curve extended to lower energies. Superposed is a histogram of the neutron energies as obtained in this experiment. Curve C is a plot of the inelastic cross section of Xe as a function of energy. Curve B, the product of curve C and curve A at each point, represents the star yield of xenon as a function of the incident neutron energy.

Table X

Classification of nonmeson events resulting from bombardment of xenon by 300-Mev neutrons

Two-Prong Stars -- Total 136

<u>Identification</u>	<u>Number observed</u>	<u>Number of prongs</u>	
		<u>T > 15</u>	<u>T > 50</u>
U, R	11	-	-
HE ³ or HE ⁴ , R	2	2	2
H ³ or HE ³ , R	4	3	1
d, R	15	10	5
d or H ³ , R	6	1	-
p, R	98	81	56

Three-Prong Stars -- Total 76

<u>Identification</u>	<u>Number observed</u>	<u>Number of prongs</u>	
		<u>T > 15</u>	<u>T > 50</u>
p, p, U	1	1	-
H ³ or HE ³ , d or H ³ , R	1	-	-
U, U, R	1	-	-
p, p, R	30	44	27
p, d, R	11	14	10
d, U, R	4	2	1
p, U, R	12	9	4
p, H ³ or HE ³ , R	4	4	1
p, d or H ³ , R	1	-	-
p, HE ³ or HE ⁴ , R	6	10	4

Four-Prong Stars -- Total 32

<u>Identification</u>	<u>Number observed</u>	<u>Number of prongs</u>	
		<u>T > 15</u>	<u>T > 50</u>
p, p, p, d	1	1	-
p, p, d or H ³ , R	1	1	-
p, d, d or H ³ , R	1	1	1

Table X (cont.)

Four-Prong Stars -- Total 32 (cont.)

<u>Identification</u>	<u>Number observed</u>	<u>Number of prongs</u>	
		<u>T > 15</u>	<u>T > 50</u>
p, p, p, p	1	2	1
d, d, p, R	1	2	1
p, d, U, R	1	2	1
p, HE ³ , HE ³ or HE ⁴ , R	1	2	-
p, p, d, R	3	6	3
p, p, p, R	6	13	4
p, p, U, R	2	2	-
p, p, H ³ or HE ³ , R	3	4	2
HE ³ or HE ⁴ , U, U, R	1	1	-
p, d or H ³ , U, R	2	1	-
p, p, HE ³ or HE ⁴ , R	2	5	-
p, H ³ or HE ³ , U, R	3	2	1
p, d or H ³ , HE ³ or HE ⁴ , R	3	4	2

Five-Prong Stars -- Total 10

<u>Identification</u>	<u>Number observed</u>	<u>Number of prongs</u>	
		<u>T > 15</u>	<u>T > 50</u>
p, p, p, p, H ³ or d	1	1	1
p, H ³ or HE ³ , H ³ or HE ³ , d or H ³ , d or H ³	1	1	-
U, U, U, R, d or H ³	1	1	-
p, p, p, d or H ³ , R	2	3	2
p, p, U, d or H ³ , R	1	2	1
p, U, d or H ³ , H ³ , d or H ³	1	1	1
p, p, U, U, R	1	2	1
d, p, R, R, HE ³ or HE ⁴	1	2	-
p, R, H ³ or HE ³ , HE ³ or HE ⁴ , HE ³ or HE ⁴ ,	1	2	-

Table X (cont.)

Six-Prong Stars -- Total 3

<u>Identification</u>	<u>Number observed</u>	<u>Number of prongs</u>	
		<u>T > 15</u>	<u>T > 50</u>
p, p, U, U, R, R	1	1	1
p, p, U, H ³ or HE ³ , HE ³ or HE ⁴ , HE ³ or HE ⁴ ,	1	3	-
p, p, p, R, U, d or H ³	1	1	-

Key: p = proton, d = deuteron, H³ = tritium, R = residual,
U = unclassified. The unclassified category contains all
particles for which the dip angle α exceeds 60°.

As a check on the validity of this assumption the numbers of prongs found in the different angular regions of Φ are given below.

(1) Mesons

Azimuthal angle, Φ			
<u>$0^\circ - 60^\circ$</u>	<u>$120^\circ - 180^\circ$</u>	<u>$180^\circ - 240^\circ$</u>	<u>$300^\circ - 360^\circ$</u>
16	17	21	19

(2) Prongs not Associated with Mesons

Azimuthal angle, Φ			
<u>$0^\circ - 60^\circ$</u>	<u>$120^\circ - 180^\circ$</u>	<u>$180^\circ - 240^\circ$</u>	<u>$300^\circ - 360^\circ$</u>
77	78	68	69

The numbers of prongs occurring in each interval of Φ given above are equal to within the statistical error of the experiment. In addition, all mesons with dip angles greater than 60° were recorded and a total number of 10 mesons was found. The number to be expected on the basis of the mathematical formulation of azimuthal symmetry was 11.

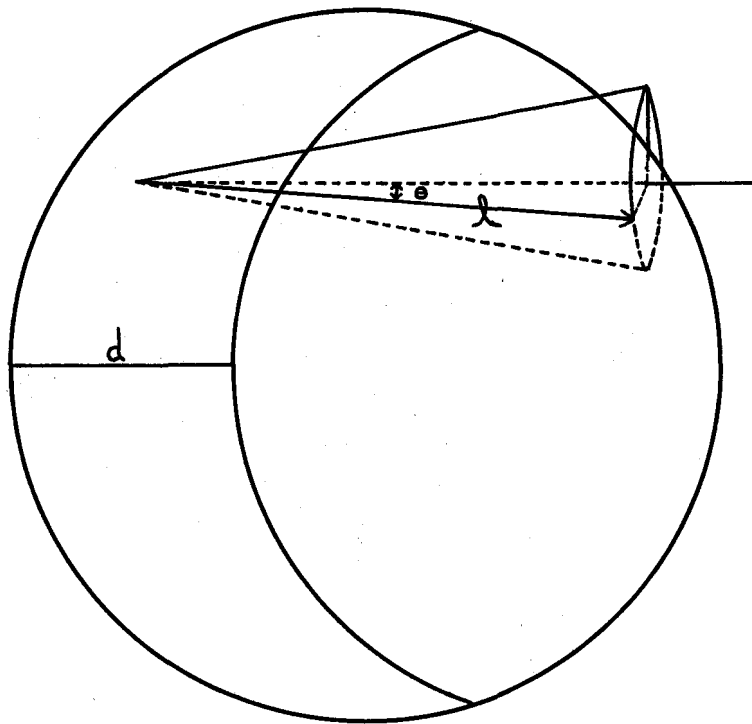
ACKNOWLEDGMENTS

Sincere thanks are due to Dr. Wilson M. Powell for his advice and encouragement during the course of this experiment.

Others who rendered valuable assistance were John B. Elliott, Dr. Stephen Gasiorowicz, Dr. Peter Moulthrop, Larry Oswald, Dr. George Saphir, and Joe Wenzel.

This work was done under the auspices of the U.S. Atomic Energy Commission.

APPENDIX I



MU-12387

Fig. A. Diagram of the nucleus with the zone for meson production, as defined by d , and the cone for meson emission at a given angle θ as defined by l . Further description given on the following page.

Relations on which computations are based are as follows..

$$d: d = \lambda_n = \frac{1}{\rho \sigma}, \quad \rho = \frac{A}{\frac{4}{3} \pi r_o^3 A}, \quad \sigma = \frac{\{(A-Z) \sigma_{nn} + Z \sigma_{np}\}}{A}$$

$$\lambda_n = \frac{4}{3} \pi r_o^3 A \left\{ (A-Z) \sigma_{nn} + Z \sigma_{np} \right\}^{-1} \quad (A-1)$$

From the values of σ_{nn} and σ_{np} at 300 Mev, the interaction mean free path for the incident neutron has a value of $4.1 \cdot 10^{-13}$ cm. A value of the mean free path of $4.0 \cdot 10^{-13}$ cm, as used in the optical model by S. Fernbach, was found to give satisfactory agreement with experiment for an incident-neutron energy of 280 Mev.

$$V_Z: V_Z = \pi R^3 G \left\{ 1 - \frac{G^2}{12} \right\}, \quad G = \frac{\lambda_n}{R} \quad (A-2)$$

V_Z represents the volume of the nucleus in which meson production can occur. R is the nuclear radius.

$$\lambda_a: \lambda_a = \frac{2}{L^2} \cdot \left\{ \frac{1+L}{2+L} \right\}^2 \cdot \frac{1}{(0.52)}, \quad L = T_\pi / m_\pi c^2, \quad \ell = k \lambda_a \quad (A-3)$$

$k = 0.64$

λ_a represents the interaction mean free path of the meson, and the equation representing it was taken from the results of a partial-wave analysis by D. Stork.¹⁸ The value of k was chosen so that more than 50% of the mesons would traverse the distance ℓ (Fig. A) without a collision.

$\frac{V_E}{V_Z}$: V_E is the volume of the nucleus effective for meson emission. It is less than or equal to the volume of the zone V_Z . The magnitude of the ratio of V_E/V_Z depends upon d , ℓ , and θ (Fig. A). The integration limits of the volume V_E are also determined by d , ℓ , θ . The value of the ratio V_E/V_Z was computed for each of the angles $\theta = 10^\circ$, $\theta = 30^\circ$, and the equations developed are given below:

$$\theta = 10^\circ: V_E/V_Z = \frac{\pi R^3}{4V_Z} \left[G^3 + \frac{F^3}{\cos \theta} - \frac{(F^2 - G^2)^2}{G + F \cos \theta} \right], \quad G = \frac{\lambda_n}{R}, \quad F = \frac{k \lambda_a}{R},$$

(A-4)

$$V_E/V_Z = \frac{3}{(12-G^2)(G)} \left[G^3 + \frac{F^3}{\cos \theta} - \frac{(F^2 - F^2)^2}{G + F \cos \theta} \right] (\theta = 10^\circ), \quad (A-5)$$

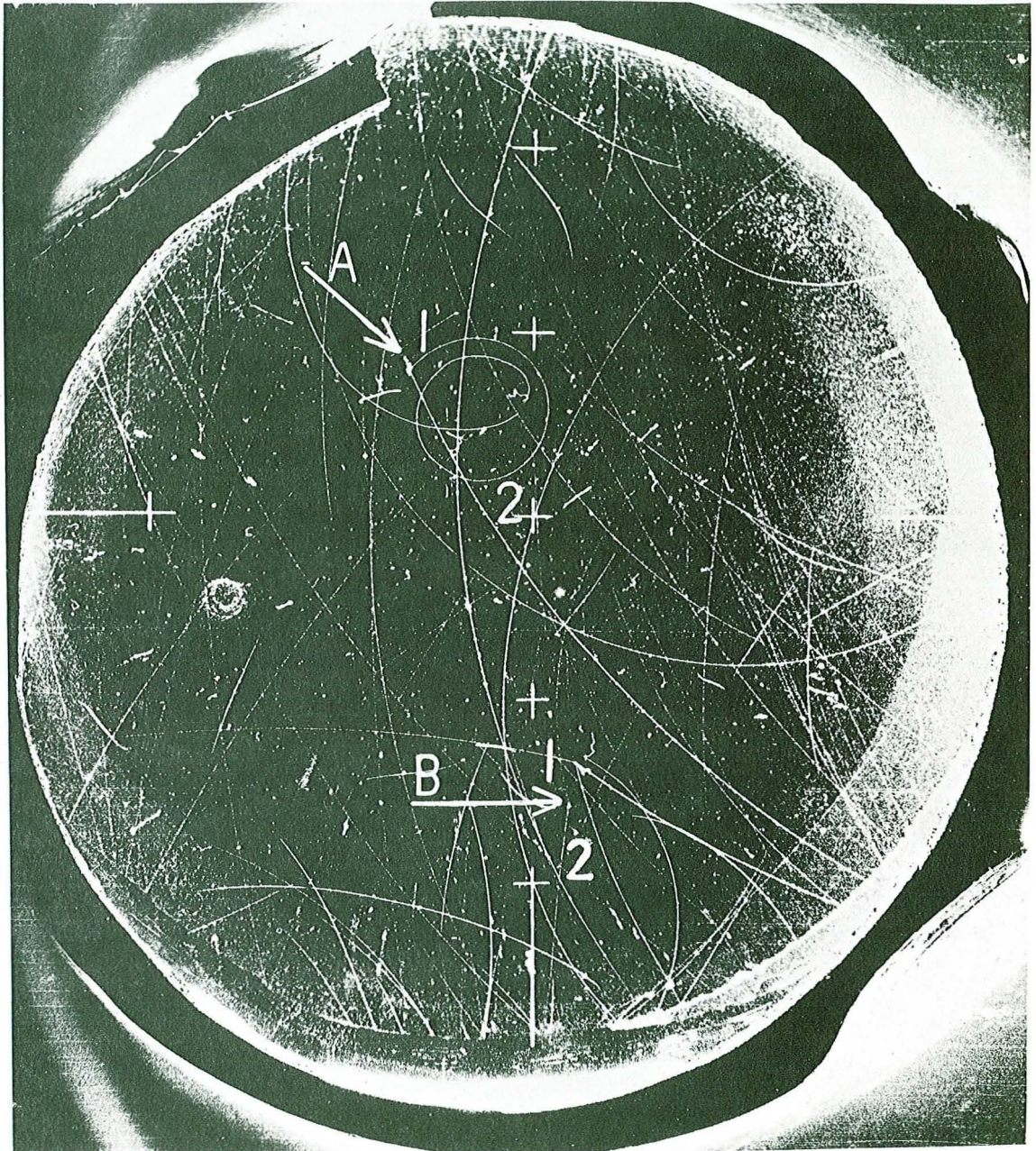
$$\theta=30^\circ V_E/V_Z = \frac{12}{(12-G^2)(G)} \left[\frac{G^3}{4} + \frac{F^3}{4 \cos \theta} - (1-G)^2 \cdot \left(\frac{2+G}{3} \right) + y_c \left\{ F^2 - 1 + \frac{y_c^2}{3} + F y_c \cos \theta \right\} \right]. \quad (A-6)$$

For $\theta = 10^\circ$ the value of λ_a is sufficiently small so that equations (A-4) and (A-5) are applicable. The calculated ratio $V_E/V_Z = 0.4$ in this case.

For $\theta = 30^\circ$ the value of λ_a is considerably increased and the formula for V_E/V_Z calculated from the altered integration limits is given by equation (A-6). The calculated ratio in this case is 0.92.

For values of θ greater than or equal to 50° the value of λ_a is sufficiently long so that the ratio $V_E/V_Z = 1.0$.

APPENDIX II



ZN-1599

Fig. B. A photograph indicating two meson events. Event "A" consists of a meson, (1), of 2-Mev energy emitted backwards, and a deuteron of 28 Mev, (2), in the forward direction. The meson in this event was observed to decay before leaving the chamber. Event "B" consists of a meson, (1), of 35-Mev energy, also emitted in the backward direction, and a high-energy deuteron, (2), of 150-Mev energy. A recoil blob is present at the origin of both events.

REFERENCES

1. Myron Knapp, Negative Pions from Neutron Bombardment of Deuterons, UCRL-2799, Nov. 1954.
2. Peter Moulthrop, Pion Production by Neutrons on Helium (Thesis), UCRL-2858, Jan. 1955.
3. Franklin C. Ford, The Production of Charged Pi Mesons by Neutrons on Oxygen, (Thesis), UCRL-2148, March 1953.
4. Melvin O. Fuller, Disintegration of Oxygen by 300-Mev Neutrons (Thesis), UCRL-2699, Sept. 1954.
5. W. Powell, Rev. Sci. Instr. 20, 403 (1949).
6. Brueckner, Hartsough, Hayward, and Powell, Phys. Rev. 75, 555 (1949).
7. Sidney Fernbach, The Scattering of High-Energy Neutrons by Nuclei and Lateral Spread of Particles in Cascade Showers, (Thesis), UCRL-1382, July 1951.
8. N. Bohr, The Penetration of Atomic Particles through Matter, second edition (Munksgaard, Copenhagen, 1953) 138-41.
9. Evans, Stier, Barnett, Phys. Rev. 90, 825 (1953).
10. S. Gasiorowicz, Phys. Rev. 93, 843 (1954).
11. W. Dudziak, Production Cross Sections for Positive and Negative Pions from Carbon Initiated by 340-Mev Protons UCRL-2564, (Thesis), 1954.
12. Bernardini, Booth, and Lederman, Phys. Rev. 93, 1277 (1951).
13. Bernardini, Booth, and Lederman, Phys. Rev. 82, 105 (1951).
14. Bernardini, Booth, and Lederman, Phys. Rev. 80, 925 (1950).
15. G. Bernardini and F. Levy, Phys. Rev. 84, 610 (1951).
16. A.M. Shapiro, Phys. Rev. 84, 1063, (1951).
17. J.F. Tracy, Phys. Rev. 91, 960 (1953).
18. H. Heckman and L. Bailey, Phys. Rev. 91, 1237, (1953).
19. D. Stork, Phys. Rev. 93, 868 (1954).
20. F. Tenney and J. Tinlot, Phys. Rev. 92, 974 (1953).
21. J. Merritt and D. Hamlin, Phys. Rev. 99, 1523 (1955).
22. K. Brueckner and K. Watson, Am. J. Phys. 21, 659 (1953).

23. Cladis, Hess, and Moyer, Phys. Rev. 87, 425 (1952).
24. McManus, Sharpe, and Gellmann, Phys. Rev. 93, 924 (1954),
and private communication to Warren Heckrotte.
25. K. LeCouteur, Proc. Phys. Soc. (London) A63, 259 (1950).
26. L. Evan Bailey, Angle and Energy Distributions of Charged Particles
from the High-Energy Nuclear Bombardment of Various Elements
(Thesis) UCRL-3334, March 1956.
27. W. Ball, Nuclear Scattering of 300-Mev Neutrons (Thesis),
UCRL-1938, Aug. 1952.
28. H. Feshbach and V. Weisskopf, Phys. Rev. 76, 1550 (1949).